Utrecht University

MSc.Thesis

Mathematical Sciences

Numerical approximation of non-monotone waves

Author:
Alina Anisimova

Supervisor:
Dr. Paul Andries Zegeling
Second reader:
Dr. Tristan van Leeuwen

February 18, 2016

Abstract

In this thesis, we numerically simulate two-phase flow in unsaturated porous media using the method of lines (MOL). The main goal of the whole research is to reproduce by means of rigorous mathematical analysis the dynamic phenomena known as infiltration overshoot that occurred during the experimental measurements of saturation, described by David DiCarlo. Specifically, such saturation profiles can be modeled using the non-equilibrium Richards' equation, which includes dynamic capillary pressure effects, essential in producing non-monotone wave solutions.
The numerical simulation procedure of MOL is split in two steps. Firstly, the spatial discretization is performed leaving the time variable continuous and secondly, a proper initial value numerical scheme is applied. The central difference scheme has been used to numerically approximate the first and second order space derivatives as part of the first step, while combination of Euler Forward and Euler Backward numerical schemes (IMEX) was introduced as part of the second step. Furthermore, in order to remove the negative effects of the original boundary conditions on the numerical solution of two-phase flow in unsaturated porous media in terms of David DiCarlo's experiments, we extend our model by including the effects of hysteresis in computation of capillary pressure function.

Contents

Acknowledgments

I would like to greatly thank my supervisor Paul Zegeling, for his intensive supervision and patience throughout the whole research during our weekly meetings. His clear explanations and inspiring discussions was a great support to me. Furthermore, I would like to acknowledge Tristan van Leeuwen as the second reader of this thesis. And last but not least, I want to thank my family for their trust and confidence in my progress.

Chapter 1

Introduction

The whole research conducted in this thesis was motivated by experiments carried out by David DiCarlo, who in 2004 published a scientific paper [4] describing the results of experimental measurements of the saturation overshoot during infiltration. The idea behind the experiments was firstly to find out what kind of behavior exhibits the two-phase fluid flow in confined uniform porous medium at different constant-flux water injections and secondly if the obtained experimental results are consistent with classical description of the fluid flow in porous media.
From the definition we know, that porous medium is the substance consisting of solid parts and voids, through which any kind of reactions take place. In order to perform his experiments, DiCarlo took initially a dry sand column and started to inject water into it. By using various experimental techniques (i.e. light transmission, etc.), he was able to see the amount of water present in various locations along the column. During the infiltration experiments, the column was vertically placed, therefore the water flow created so called infiltration profiles, which were moving downward due to the gravitational forces. Obviously, at locations where the injection took place, there was more water than anywhere else in the column, making it possible to observe certain kind of saturation profiles. According to traditional theory on fluid flow, these saturation profiles are expected to demonstrate the monotonic behavior.
DiCarlo did his experiments with certain flow rates and initial water saturations. Initially he started with small injection rates, but then he started to pour water into the sand column harder and harder, significantly increasing the injection rates. Based on the experimental results, DiCarlo was able

to observe the fact that constant-flux infiltrations into the porous medium were found to produce the saturation overshoots. But these experimentally obtained saturation overshoots were conflicting with the traditional mathematical approaches used to characterize the flow of fluid in the porous media.

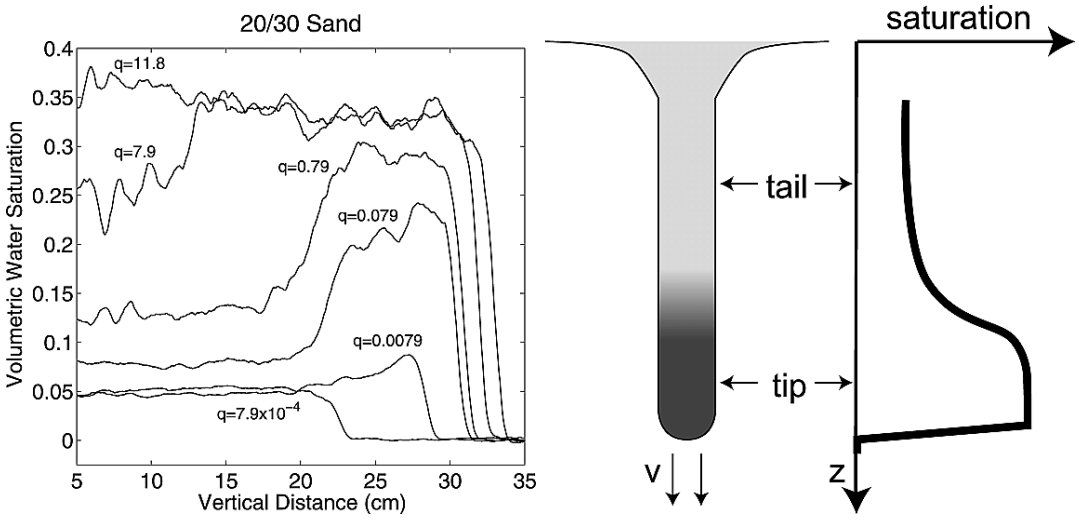

Figure 1.1: (left) Sketch of volumetric water saturation profile versus vertical distance (depth) for six different injection rates (q) obtained by DiCarlo during experimental measurements on infiltration [4]. (right) Animation of a preferential flow and corresponding saturation profile within the flow path. Saturation overshoot occurs when saturation before wetting front (tip) is greater than saturation behind the wetting front (tail).

The results of DiCarlo's experiments are illustrated in Figure 1.1, where the snapshots of measured volumetric water saturation profiles into dry sand at six different injection rates (q) are plotted over depth. At the lowest injection rate ($q = 7.9 * 10^{-4} cm/min$) and the highest one ($q = 11.8 cm/min$) monotone profiles without saturation overshoot are observed, while at all the intermediate injection rates, saturation profiles are demonstrating non-monotone or distinct plateau type behavior with saturation overshoot. Moreover, saturations at the wetting front (tip) significantly surpassing those located behind the wetting front (tail). The slight oscillations (wiggles) at the tail are likely to be experimental or measurement inaccuracies.
The main goal of our numerical investigation is to reproduce by means of rig-

orous mathematical analysis and the enhanced models including additional terms describing non-monotone fluid flow in porous media, the dynamic phenomena known as infiltration overshoot that occurred during the experimental measurements of DiCarlo described above.

Chapter 2

Modeling of unsaturated flow in porous media

2.1 Mathematical model setup

Initially we have a dry porous medium, which is filled with sand (as in experiments conducted by David DiCarlo[4]). DiCarlo performed his experiments vertically. Everything in the porous media is homogeneous (distribution of grains is quite straightforward). There are two types of fluids running in this column, which are called phases: wetting and non-wetting. The notion of wetting and non-wetting phases is relative. Throughout out this paper we refer to water as wetting phase and air as non-wetting phase. We assume that the two phases are immiscible. In particular, if we take a small volume of porous media, we would like to understand how much percentage is filled by water and air respectively in the pores.
The key issue here is to know how much percentage of water and air is occupying a certain region in the porous media. Typical equations to describe such kind of processes are called mass balance equations. Mass balance equations are stating that the mass is conserved in phase α. Mass conservation of fluid across the porous medium describes the basic principle that mass flux in minus mass flux out is equivalent to the the increase in amount stored by a medium. This means that total mass of the fluid is always conserved [5]. The partial differential equation expressing the mass conservation for both fluid phases in dimensionless setting is therefore:

$$\phi \frac{\partial S_\alpha}{\partial t} + \nabla \cdot q_\alpha = 0, \qquad \alpha \in \{w, a\}\,. \tag{2.1}$$

Here the subscript α refers to either air or water phase respectively, q_α is Darcy's velocity for each of the phases and ϕ is porosity, which takes the values:

$$0 \leq \phi \leq 1.$$

According to generalized Darcy's law:

$$q_\alpha = -\frac{K_\alpha(S_\alpha)}{\mu_\alpha} \cdot \nabla(p_\alpha - \rho_\alpha g z). \tag{2.2}$$

Here K_α stands for unsaturated hydraulic conductivity of the phase α, which depends on its saturation S_α. Constant g is the gravitational acceleration, p_α is phase pressure, μ_α is dynamic viscosity of phase α and ρ_α is phase density. Here z is vertical spatial variable which is oriented positively upwards and oppositely to the direction of gravity. Darcy's law states that velocity is proportional to pressure gradient and proportionality factor is represented by a function. The negative sign in the equation (2.2) mathematically allows the fluid flow move in the right direction, meaning from high hydraulic head to low hydraulic head. If flow moves in the positive direction and the gradient is negative, the relation needs to have a negative sign. Darcy's law application allows hydraulic conductivity to be determined, therefore K_α can be written as:

$$K_\alpha = K \cdot k_{r\alpha}(S_\alpha), \tag{2.3}$$

where K denotes the intrinsic permeability of the porous medium and $k_{r\alpha}$ stands for the relative permeability of the given phase α, which takes values between 0 and 1, i.e:

$$0 \leq k_{r\alpha}(S_\alpha) \leq 1.$$

Substituting the expression (2.3) into (2.2) results in:

$$q_\alpha = -K\frac{k_{r\alpha}(S_\alpha)}{\mu_\alpha} \cdot \nabla(p_\alpha - \rho_\alpha g z). \tag{2.4}$$

By using the relation for mobility phase α:

$$\lambda_\alpha = \frac{k_{r\alpha}}{\mu_\alpha}, \tag{2.5}$$

generalized Darcy's law (2.4) can be reduced to the following form:

$$q_\alpha = -K\lambda_\alpha(S_\alpha) \cdot \nabla(p_\alpha - \rho_\alpha g z). \tag{2.6}$$

Combining the mass balance equation and Darcy's law for each of the phases results in:

$$\phi \frac{\partial S_\alpha}{\partial t} = \nabla \left[K \frac{k_{r\alpha}(S_\alpha)}{\mu_\alpha} \cdot \nabla \left(p_\alpha - \rho_\alpha g z \right) \right], \tag{2.7}$$

$$p_\alpha = P(S_\alpha), \tag{2.8}$$

where function P denotes the equilibrium pressure or so called static pressure. Now we have four unknowns (two phase pressures and two phase saturations) and only two equations. If we add the amount of air in one location, the percentage occupied by air and the percentage occupied by water together fill the whole space of the pores. Since the two fluids occupy the whole pore space, so we receive the additional algebraic relation:

$$S_a + S_w = 1. \tag{2.9}$$

Engineers are able to measure the pressures into the both phases, i.e they are able to establish differences between two phases by relating to the amount of water saturation. Because of the existence of interfacial tension, the pressure of non-wetting phase is higher than the pressure in wetting one:

$$p_o - p_w = P_c(S). \tag{2.10}$$

Here P_c denotes the capillary pressure in two-phase flow. Capillary pressure relationship represents a function of saturation, which depends on the direction of saturation change. It is a monotonic function, which can be measured experimentally and it is always positive. Relationship (2.10) holds only under equilibrium conditions and is called static capillary pressure. Therefore such a mathematical model is called an equilibrium model.

2.2 The Richards' equation

As the starting point in simulation of infiltration experiments performed by DiCarlo in [4], we consider the Richards' equation (Richards, 1931; Bear, 1972; Kutilek & Nielsen, 1994), which is usually used for modeling of unsaturated fluid flow in porous media.

Using relation (2.9), and assuming that total flow $q = q_w + q_a$ we arrive in 1D at:

$$\frac{\partial}{\partial z} q = \frac{\partial}{\partial z} \left(q_w + q_o \right) = 0 \Longrightarrow q = 0.$$

Using this observation and the relations mentioned above, we introduce the diffusivity function $D\left(S\right) = f\left(S\right) \left| P_c^{'}(S) \right|$. This allows us to reduce the two-phase model (2.7) to one equation in terms of only water saturation. Such equation is called the Richards' equation:

$$\phi \frac{\partial S}{\partial t} + \frac{\partial}{\partial z} \left(q f(S) + K \lambda_a(S) f(S) (\rho_w - \rho_a) g \right) + \\ + \frac{\partial}{\partial z} \left(\lambda_a f(S) \frac{\partial}{\partial z} |P_c^{'}| \right) = 0. \tag{2.11}$$

Since we do not want our model to be ill-posed, it is required that the diffusivity term in (2.11) is always non-negative. Therefore we impose a modules sign on $P_c^{'}(S)$. Here we assume that the following inequality is satisfied:

$$0 \leq P_c^{'}(S) < \infty.$$

In equation (2.11), $S = S_w$ and after Brooks and Corey, 1964 [20], f represents the fraction flow function:

$$f(S) = \frac{\lambda_w}{\lambda_w + \lambda_a}, \tag{2.12}$$

where λ_w is the water mobility, which reads as:

$$\lambda_w = \frac{K}{\mu_w} k_{rw}, \tag{2.13}$$

and λ_a is the air mobility, which reads as:

$$\lambda_a = \frac{K}{\mu_a} k_{ra}. \tag{2.14}$$

Since the relative water permeability k_{rw} equals to:

$$k_{rw} = S^{\frac{2+3\lambda}{\lambda}}, \tag{2.15}$$

and the relative air permeability k_{ra} is equal to:

$$k_{ra} = (1 - S)^2(1 - S^{\frac{2+\lambda}{\lambda}}). \tag{2.16}$$

The fractional flow function (2.12) is written as:

$$f(S) = \frac{S^{\frac{2+3\lambda}{\lambda}}}{S^{\frac{2+3\lambda}{\lambda}} + M(1 - S)^2(1 - S^{\frac{2+\lambda}{\lambda}})}, \tag{2.17}$$

where M denotes the mobility ratio of two given phases:

$$M = \frac{\mu_w}{\mu_a}. \tag{2.18}$$

2.3 The non-equilibrium Richards' equation

In the previous section we assumed that equilibrium conditions are being held while modeling the two-phase flow in unsaturated porous media. Essentially, the fluids pressure difference relation (2.10) holds only when both fluids are at rest. Otherwise, the capillary pressure function depends on the rate of change of saturation and relation (2.10) obviously does not hold anymore. That is the reason why we call the equation (2.11) the equilibrium Richards' equation or simply equilibrium model. Standard equilibrium models can only produce monotone wave profiles. From infiltration experiments described by DiCarlo, we know that he injected water in the sand porous medium at different flux rates and made his measurements while the processes occurred. This means that at relatively high injection rates, the processes within the column were taking place much faster compared to the ones performed at relatively low fluxes. Therefore we need to include non-equilibrium assumptions in terms of the dynamical effects on capillary pressure function[6, 9]. To account for the dynamics into the processes, a non-equilibrium approach was proposed by S.M. Hassanizadeh and W.Gray in [5] where dynamic capillary pressure may take the following form:

$$p_o - p_w = P_c(S) + \tau \frac{\partial S}{\partial t}. \tag{2.19}$$

Here τ is the dimensionless damping coefficient, which is always positive. Essentially non-equilibrium assumption is the reason why time dependency

is added in relation (2.19). Now using again the definition of the diffusivity function $D(S) = f(S)|P_c^{'}(S)|$ and non-equilibrium relation (2.19), we re-write the equilibrium Richards' equation (2.11) in its non-equilibrium form:

$$\phi\frac{\partial S}{\partial t} + \frac{\partial}{\partial z}\left[qf(S)\right] + \frac{\partial}{\partial z}\left[\lambda_\sigma f(S) g\Delta\rho\right] =$$
$$= \frac{\partial}{\partial z}\left[\lambda_\sigma f(S)|P_c^{'}(S)|\frac{\partial S}{\partial z}\right] + \tau\frac{\partial}{\partial z}\left[\lambda_\alpha f(S)\frac{\partial^2 S}{\partial z \partial t}\right]. \qquad (2.20)$$

The governing equation (2.20) represents the full form of the non-equilibrium Richards' equation, which we will use to numerically approximate the saturation overshoots observed in infiltration experimental measurements of DiCarlo.

Chapter 3

Numerical simulation of two-phase flow in porous media

This chapter introduces the numerical approximation technique called the method of lines (MOL) applied to approximate two-phase flow governing equation in porous media. In particular we will focus our attention on the numerical method used as part of MOL implementation, which is called Implicit-Explicit (IMEX). Here we will discuss the reason why a combination of Euler-Forward and Euler-Backward numerical schemes is more advantageous compared to separately applied explicit or implicit scheme. Firstly we will apply the method of lines in combination with IMEX to simplified a model in order to make it more easy to analyze the behavior and convergence of obtained solutions and then we apply the same technique to the full model, which is determined by a specific choice of constant parameters and functions suitable for experiments.

3.1 Method of lines

Let's consider the following partial differential equation:

$$\frac{\partial S}{\partial t} = d\frac{\partial^2 S}{\partial z^2} + \frac{\partial f(S)}{\partial z} + \tau\frac{\partial^3 S}{\partial t \partial z^2},\ z \in [z_l, z_r],\ t \in [0, T], \tag{3.1}$$

with boundary conditions:

$$S(z_l, t) = S_- \text{ and } S(z_r, t) = S_+,\ (0 \leq S_- < S_+ \leq 1)\,, \tag{3.2}$$

and initial conditions:

$$S(z,0) = S_- + \frac{1}{2}(S_+ - S_-)(1 + \tanh(R(z - z_0))). \tag{3.3}$$

One way of solving such a time-dependent PDE numerically is to use the method of lines (MOL). The idea behind this technique is that the spatial (in space) and temporal (in time) discretizations (approximations) are done in two separate steps. At first step, we leave the time variable continuous and only discretize the spatial derivatives.

$$\begin{cases} \dot{S}_i = d\frac{S_{i+1}-2S_i+S_{i-1}}{(\Delta z)^2} + \frac{S_{i+1}^2-S_{i-1}^2}{4\Delta z} + \tau\frac{\dot{S}_{i+1}-2\dot{S}_i+\dot{S}_{i-1}}{(\Delta z)^2}, \\ \qquad i = 2,\ldots,I-1, \end{cases} \tag{3.4}$$

where

$$\dot{S}_1 = 0,\ S_1(0) = S_-,\ \dot{S}_I = 0 \text{ and } S_I(0) = S_+,$$

and initial function

$$\begin{cases} S_i(0) = S_- + \frac{1}{2}(S_+ - S_-)(1 - \tanh(R(z_i - z_0))), \\ \qquad i = 2,\ldots,I-1. \end{cases}$$

Here the dot above S, denotes its time derivative. At this point, approximation of the exact solution at grid point z_i for all time is given by:

$$S_i(t) \approx S(z_i,t), \quad t > 0.$$

The spatial step $\Delta z = \frac{1.4}{I-1}$ and each spatial grid point is given as $z_i = \frac{i-1}{I-1}\cdot 1.4$, where $i \in \{i,\ldots,I\}$, with I being the number of spatial grid points.
After this step we end up with the dynamical system of time dependent ordinary differential equations (ODEs).

$$\begin{cases} M\dot{\vec{S}} = D\vec{S} + \vec{g}(\vec{S}), \\ \vec{S}(0) = \vec{S}^1, \end{cases}$$

where

$$\vec{S}^1 = \begin{pmatrix} S_- \\ S_2(0) \\ S_3(0) \\ \vdots \\ S_{I-1}(0) \\ S_+ \end{pmatrix}, \vec{S} = \begin{pmatrix} S_- \\ S_2(t) \\ S_3(t) \\ \vdots \\ S_{I-1}(t) \\ S_+ \end{pmatrix} \text{ and } \vec{g}(\vec{S}) = \begin{pmatrix} 0 \\ \frac{S_3^2-S_1^2}{4\Delta z} \\ \frac{S_4^2-S_2^2}{4\Delta z} \\ \vdots \\ \frac{S_I^2-S_{I-2}^2}{4\Delta z} \\ 0 \end{pmatrix}.$$

Here M and D are the tridiagonal matrices which have the following structure:

$$M = \begin{pmatrix} 1 & 0 & 0 & 0 & \cdots & 0 \\ \frac{-\tau}{(\Delta z)^2} & 1+\frac{2\tau}{(\Delta z)^2} & \frac{-\tau}{(\Delta z)^2} & 0 & \cdots & 0 \\ 0 & \frac{-\tau}{(\Delta z)^2} & 1+\frac{2\tau}{(\Delta z)^2} & \frac{-\tau}{(\Delta z)^2} & \cdots & 0 \\ 0 & 0 & \ddots & \ddots & \ddots & 0 \\ 0 & 0 & 0 & \frac{-\tau}{(\Delta z)^2} & 1+\frac{2\tau}{(\Delta z)^2} & \frac{-\tau}{(\Delta z)^2} \\ 0 & 0 & 0 & 0 & 0 & 1 \end{pmatrix},$$

$$D = \begin{pmatrix} 0 & 0 & 0 & 0 & \cdots & 0 \\ \frac{d}{(\Delta z)^2} & \frac{-2d}{(\Delta z)^2} & \frac{d}{(\Delta z)^2} & 0 & \cdots & 0 \\ 0 & \frac{d}{(\Delta z)^2} & \frac{-2d}{(\Delta z)^2} & \frac{d}{(\Delta z)^2} & \cdots & 0 \\ 0 & 0 & \ddots & \ddots & \ddots & 0 \\ 0 & 0 & 0 & \frac{d}{(\Delta z)^2} & \frac{-2d}{(\Delta z)^2} & \frac{d}{(\Delta z)^2} \\ 0 & 0 & 0 & 0 & 0 & 0 \end{pmatrix}$$

At the second step of MOL, a proper initial value numerical scheme is applied to solve the system of time dependent ODEs. Here we are going to use an Implicit – Explicit method, which we will discuss in the next section.

3.2 Implicit - Explicit method (IMEX)

Equation (3.1) contains both stiff and nonlinear terms. Here stiff term is presented by a diffusion expression. Implicit schemes are considered to be more suitable for solving PDEs with stiff terms rather then implicit schemes as they give a possibility to use a large time-step. Explicit schemes require the use of impractically small time step in order to produce the stable numerical solution at a cost of long computation time. Oppositely, if we treat nonlinear term with an implicit scheme, it will require solving a nonlinear system of equations during each time step, which is very time consuming and practically inefficient.
An appropriate mix of implicit and explicit schemes may help to avoid downsides of both schemes making an IMEX scheme to be an advantageous choice. In the implementation of IMEX, the diffusion term is computed by an implicit scheme avoiding requirement to use a small time step, while the nonlinear

term is calculated using an explicit scheme without need to solve a nonlinear system of equations at every time step.
Taking into account the previous arguments we now can apply a combination of implicit and explicit finite difference methods to the system of time-dependent ODEs we received in the previous steps. Consequently at the second step of method of lines we apply the IMEX method:

$$\begin{cases} M\frac{\vec{S}^{n+1}-\vec{S}^{n}}{\Delta t} &= D\vec{S}^{n+1}+\vec{g}\left(\vec{S}^{n}\right), \\ \vec{S}^{1} \text{ given,} \end{cases} \tag{3.10}$$

$$\Rightarrow \begin{cases} \left(M-\Delta tD\right)\vec{S}^{n+1} &= M\vec{S}^{n}+\Delta t\vec{g}\left(\vec{S}^{n}\right), \\ \vec{S}^{1} \text{ given,} \end{cases}$$

$$\Rightarrow \begin{cases} \vec{S}^{n+1} &= \left(M-\Delta tD\right)^{-1}\left(M\vec{S}^{n}+\Delta t\vec{g}\left(\vec{S}^{n}\right)\right), \\ \vec{S}^{1} \text{ given.} \end{cases}$$

In the numerical computing environment Matlab, the calculation of a matrix inverse is executed by using the matrix division operator \ [19].

3.3 Stability of the IMEX method

There are many IMEX methods available. In our numerical approximations we are going to consider Euler Forward-Euler Backward as the chosen IMEX method [17].
Lets consider the following PDE:

$$\frac{\partial s}{\partial t} = H(s(t),t)+G(s(t),t). \tag{3.11}$$

Here H represents a nonstiff term suitable for applying the explicit scheme (Euler Forward), while G represents a stiff term suitable for applying the implicit scheme (Euler Backward).
The splitting method or the IMEX scheme is given by:

$$s^{n+1} = s^{n}+\Delta tH(s^{n},t^{n})+(1-\theta)\Delta tG(s^{n},t^{n})+\theta\Delta tG(s^{n+1},t^{n+1}), \tag{3.12}$$

where Δt is the uniform temporal step size and s^n are numerical approximations, $s^n \approx s(t^n)$ at the time step levels $t^n = n\Delta t$.

In order to be able to analyze the stability of the applied IMEX scheme, lets consider the following complex scalar test equation:

$$\frac{ds}{dt} = \lambda_H s(t) + \lambda_G s(t), \tag{3.13}$$

where $\lambda' s$ are the eigenvalues of H and G after linearization. Combining the test function (3.13) with (3.12) results in:

$$s^{n+1} = s^n + \Delta t \lambda_h s^n + (1-\theta)\Delta t \lambda_G s^n + \theta \Delta t \lambda_G s^{n+1}. \tag{3.14}$$

After bringing the terms containing s^{n+1} to the left hand side of the equation and bringing the other terms to the right hand side gives the following expression:

$$(1 - \theta \Delta t \lambda_G) s^{n+1} = (1 + \Delta t \lambda_H + (1-\theta)\Delta t \lambda_G) s^n, \tag{3.15}$$

or equivalently:

$$s^{n+1} = \frac{(1 + \Delta t \lambda_H + (1-\theta)\Delta t \lambda_G)}{(1 - \theta \Delta t \lambda_G)} s^n. \tag{3.16}$$

Therefore, the stability of IMEX-θ scheme requires:

$$\left| \frac{(1 + \Delta t \lambda_H + (1-\theta)\Delta t \lambda_G)}{(1 - \theta \Delta t \lambda_G)} \right| \leq 1. \tag{3.17}$$

From now on, we are going to apply the IMEX method with $\theta = 1$. In this case the stability requirement of the applied IMEX scheme is fulfilled if the following two conditions are satisfied:

$$|1 - \Delta t \lambda_G| \geq 1 \text{ and } |1 + \Delta t \lambda_H| \leq 1. \tag{3.18}$$

In other words, the stability conditions (3.18) imply that the IMEX scheme with $\theta = 1$ is stable if the explicit part satisfies the stability requirement of the Euler Forward (Explicit method) and the implicit part satisfies the stability requirement for the Euler backward (Implicit method). Recall, that the stability requirement of Euler Forward is satisfied when $|1+\Delta t \lambda| \leq 1$, i.e. eigenvalues should have real part negative $Re(\lambda) < 0$ or equivalently, eigenvalues must stay inside of the circle in the left half plane while the stability condition of Euler Backward condition requires $|\frac{1}{1-\Delta t \lambda}| < 1$, i.e. eigenvalues must stay out of the circle in right half plane.
In general, the stability conditions (3.18) are not true for $\theta \neq 1$. Consideration of stability analysis for case $\theta \neq 1$ is not in the scope of this thesis. For detailed analysis on stability requirements we refer to [17].

3.4 Method of lines applied to the non-equilibrium Richards' equation

In this section we are going to demonstrate the application of the Method of Lines in combination with the IMEX scheme to the non-equilibrium Richards' equation, used to approximate the experiments of the two-phase flow in porous media with distinguishing features observed by DiCarlo. In the previous chapter we have specified, that the full governing nonlinear PDE, which we are going to approximate, is given by:

$$\phi\frac{\partial S}{\partial t}+\frac{\partial}{\partial z}\left[qf(S)\right]+\frac{\partial}{\partial z}\left[\lambda_\sigma f(S)g\Delta\rho\right]= \\ =\frac{\partial}{\partial z}\left[\lambda_\sigma f(S)|P_c^{'}(S)|\frac{\partial S}{\partial z}\right]+\tau\frac{\partial}{\partial z}\left[\lambda_\alpha f(S)\frac{\partial^2 S}{\partial z\partial t}\right].$$

For simplicity, we will put all the terms containing spatial and mixed derivatives on the right-hand side of the equation, while keeping the term containing temporal derivative on the left-hand side and re-write equation (2.20) in general form as:

$$\phi\frac{\partial S}{\partial t}=\frac{\partial}{\partial z}\left(D(S)\frac{\partial S}{\partial z}\right)+\tau\left(\frac{\partial}{\partial z}\left(M\left(S\right)\frac{\partial^2 S}{\partial z\partial t}\right)\right)-q\frac{\partial f(S)}{\partial z}-\frac{\partial}{\partial z}\left(G\left(S\right)\right). \tag{3.19}$$

Furthermore, as the third and fourth terms on the right-hand side, which are represented by the fractional flow function and gravity terms respectively, contain both first-order derivatives, we can combine them in one expression and equivalently rewrite equation (3.19) as:

$$\phi\frac{\partial S}{\partial t}=-\frac{\partial}{\partial z}g(S)+\frac{\partial}{\partial z}\left(D(S)\frac{\partial S}{\partial z}\right)+\tau\left(\frac{\partial}{\partial z}\left(M(S)\frac{\partial^2 S}{\partial z\partial t}\right)\right), \tag{3.20}$$

where introduced the function $g(S)=-(qf(S)+G(S))$.
As the first step of MOL, we start by discretizing the spatial derivatives. This means we approximate the exact solution only at spatial grid points z_i, keeping the time continuous and we do so by choosing an appropriate finite difference scheme from many discretization options available.
At the second step, we apply the IMEX-θ integration scheme with $\theta=1$. The first term $g(s)$ on the right hand side of (3.20) is nonlinear, therefore

is suitable for explicit time integration. The other two terms, $D(S)\frac{\partial^2 S}{\theta z^2}$ and $M(S)\frac{\partial^3 S}{\partial z^2 \partial t}$, are stiff and hence suitable for implicit integration.
It is important to recognize that the second and third term on the right hand side of (3.20) are both dependent on the saturation S. This means that applying the IMEX method directly to the system of time dependent ODEs, which we receive from the first step, would mean to solve the system of nonlinear equations at each time step. In order to avoid it, we compute both terms at step t^n instead of time step t^{n+1}.
The left-hand side term of equation (3.20) which contains time derivative, is approximated by:

$$\left.\frac{\partial S}{\partial t}\right|_i^n \approx \frac{(S_i^{n+1}) - (S_i^n)}{\Delta t}$$

In order to discretize the first-order derivatives of the first term on the right hand-side of equation (3.20), we use a second-order central finite difference approximation and then we apply explicit time integration (Euler-Forward):

$$\left.\frac{\partial g}{\partial z}\right|_i^n \approx \frac{g(S_{i+1}^n) - g(S_{i-1}^n)}{2\Delta z}$$

The second term on the right-hand side of equation (3.20) represents the nonlinear diffusion term. Again we apply the central spatial discretization to approximate the second order derivatives:

$$\begin{aligned}
\left.\frac{\partial}{\partial z}\left(D\left(S\right)\frac{\partial S}{\partial z}\right)\right|_i^n \approx & \frac{D\left(S_{i+\frac{1}{2}}^n\right)\left.\frac{\partial S}{\partial z}\right|_{i+\frac{1}{2}}^{n+1} - D\left(S_{i-\frac{1}{2}}^n\right)\left.\frac{\partial S}{\partial z}\right|_{i-\frac{1}{2}}^{n+1}}{\Delta z} \\
\approx & \frac{D\left(S_{i+\frac{1}{2}}^n\right)\left(S_{i+1}^{n+1} - S_i^{n+1}\right) - D\left(S_{i-\frac{1}{2}}^n\right)\left(S_i^{n+1} - S_{i-1}^{n+1}\right)}{(\Delta z)^2} \\
\approx & \frac{D\left(S_{i+1}^n\right) + D\left(S_i^n\right)}{2}\frac{S_{i+1}^{n+1} - S_i^{n+1}}{(\Delta z)^2} - \frac{D\left(S_i^n\right) + D\left(S_{i-1}^n\right)}{2}\frac{S_i^{n+1} - S_{i-1}^{n+1}}{(\Delta z)^2} \\
\approx & \left(\frac{D(S_{i+1}^n)}{2(\Delta z)^2} + \frac{D(S_i^n)}{2\Delta z)^2}\right)S_{i+1}^{n+1} - \left(\frac{D(S_{i+1}^n)}{2(\Delta z)^2} + \frac{D(S_i^n)}{(\Delta z)^2} + \frac{D(S_{i-1}^n)}{2(\Delta z)^2}\right)S_i^{n+1} \\
& + \left(\frac{D(S_i^n)}{2(\Delta z)^2} + \frac{D(S_{i-1}^n)}{2(\Delta z)^2}\right)S_{i-1}^{n+1},
\end{aligned}$$

where $D(S) =$

$$\frac{\frac{K}{\mu_o}(1-S)^2\left(1-S^{\frac{2+\lambda}{\lambda}}\right)S^{\frac{2+3\lambda}{\lambda}}}{S^{\frac{2+3\lambda}{\lambda}}+\frac{\mu_w}{\mu_o}(1-S)^2\left(1-S^{\frac{2+\lambda}{\lambda}}\right)}\left|\frac{P_d}{\lambda}S^{-\frac{\lambda+1}{\lambda}}\right| = \frac{\frac{K}{\mu_o}\frac{P_d}{\lambda}(1-S)^2\left(1-S^{\frac{2+\lambda}{\lambda}}\right)S^{\frac{2\lambda+1}{\lambda}}}{S^{\frac{2+3\lambda}{\lambda}}+\frac{\mu_w}{\mu_o}(1-S)^2\left(1-S^{\frac{2+\lambda}{\lambda}}\right)}.$$

Hence the full discretization of diffusion term $D(S)$ is the following:

$$\begin{aligned}
D(S) =& \frac{\frac{\frac{K}{\mu_o}\frac{P_d}{\lambda}(1-S_{i+1})^2\left(1-S_{i+1}^{\frac{2+\lambda}{\lambda}}\right)Si+1^{\frac{2\lambda+1}{\lambda}}}{S_{i+1}^{\frac{2+3\lambda}{\lambda}}+\frac{\mu_w}{\mu_o}(1-S_{i+1})^2\left(1-S_{i+1}^{\frac{2+\lambda}{\lambda}}\right)} + \frac{\frac{K}{\mu_o}\frac{P_d}{\lambda}(1-S_i)^2\left(1-S_i^{\frac{2+\lambda}{\lambda}}\right)Si^{\frac{2\lambda+1}{\lambda}}}{S_i^{\frac{2+3\lambda}{\lambda}}+\frac{\mu_w}{\mu_o}(1-S_i)^2\left(1-S_i^{\frac{2+\lambda}{\lambda}}\right)}}{2}\frac{S_{i+1}-S_i}{(\Delta z)^2} \\
& - \frac{\frac{\frac{K}{\mu_o}\frac{P_d}{\lambda}(1-S_i)^2\left(1-S_i^{\frac{2+\lambda}{\lambda}}\right)Si^{\frac{2\lambda+1}{\lambda}}}{S_i^{\frac{2+3\lambda}{\lambda}}+\frac{\mu_w}{\mu_o}(1-S_i)^2\left(1-S_i^{\frac{2+\lambda}{\lambda}}\right)} + \frac{\frac{K}{\mu_o}\frac{P_d}{\lambda}(1-S_{i-1})^2\left(1-S_{i-1}^{\frac{2+\lambda}{\lambda}}\right)Si-1^{\frac{2\lambda+1}{\lambda}}}{S_{i-1}^{\frac{2+3\lambda}{\lambda}}+\frac{\mu_w}{\mu_o}(1-S_{i-1})^2\left(1-S_{i-1}^{\frac{2+\lambda}{\lambda}}\right)}}{2}\frac{S_i-S_{i-1}}{(\Delta z)^2} \\
=& \frac{\frac{\frac{K}{\mu_o}\frac{P_d}{\lambda}(1-S_{i+1})^2\left(1-S_{i+1}^{\frac{2+\lambda}{\lambda}}\right)Si+1^{\frac{2\lambda+1}{\lambda}}}{S_{i+1}^{\frac{2+3\lambda}{\lambda}}+\frac{\mu_w}{\mu_o}(1-S_{i+1})^2\left(1-S_{i+1}^{\frac{2+\lambda}{\lambda}}\right)} + \frac{\frac{K}{\mu_o}\frac{P_d}{\lambda}(1-S_i)^2\left(1-S_i^{\frac{2+\lambda}{\lambda}}\right)Si^{\frac{2\lambda+1}{\lambda}}}{S_i^{\frac{2+3\lambda}{\lambda}}+\frac{\mu_w}{\mu_o}(1-S_i)^2\left(1-S_i^{\frac{2+\lambda}{\lambda}}\right)}}{2(\Delta z)^2}S_{i+1} \\
& - \frac{\frac{\frac{K}{\mu_o}\frac{P_d}{\lambda}(1-S_{i+1})^2\left(1-S_{i+1}^{\frac{2+\lambda}{\lambda}}\right)Si+1^{\frac{2\lambda+1}{\lambda}}}{S_{i+1}^{\frac{2+3\lambda}{\lambda}}+\frac{\mu_w}{\mu_o}(1-S_{i+1})^2\left(1-S_{i+1}^{\frac{2+\lambda}{\lambda}}\right)}}{2(\Delta z)^2}S_i - 2\frac{\frac{\frac{K}{\mu_o}\frac{P_d}{\lambda}(1-S_i)^2\left(1-S_i^{\frac{2+\lambda}{\lambda}}\right)Si^{\frac{2\lambda+1}{\lambda}}}{S_i^{\frac{2+3\lambda}{\lambda}}+\frac{\mu_w}{\mu_o}(1-S_i)^2\left(1-S_i^{\frac{2+\lambda}{\lambda}}\right)}}{2(\Delta z)^2}S_i \\
& - \frac{\frac{\frac{K}{\mu_o}\frac{P_d}{\lambda}(1-S_{i-1})^2\left(1-S_{i-1}^{\frac{2+\lambda}{\lambda}}\right)Si-1^{\frac{2\lambda+1}{\lambda}}}{S_{i-1}^{\frac{2+3\lambda}{\lambda}}+\frac{\mu_w}{\mu_o}(1-S_{i-1})^2\left(1-S_{i-1}^{\frac{2+\lambda}{\lambda}}\right)}}{2(\Delta z)^2}S_i \\
& + \frac{\frac{\frac{K}{\mu_o}\frac{P_d}{\lambda}(1-S_i)^2\left(1-S_i^{\frac{2+\lambda}{\lambda}}\right)Si^{\frac{2\lambda+1}{\lambda}}}{S_i^{\frac{2+3\lambda}{\lambda}}+\frac{\mu_w}{\mu_o}(1-S_i)^2\left(1-S_i^{\frac{2+\lambda}{\lambda}}\right)} + \frac{\frac{K}{\mu_o}\frac{P_d}{\lambda}(1-S_{i-1})^2\left(1-S_{i-1}^{\frac{2+\lambda}{\lambda}}\right)Si-1^{\frac{2\lambda+1}{\lambda}}}{S_{i-1}^{\frac{2+3\lambda}{\lambda}}+\frac{\mu_w}{\mu_o}(1-S_{i-1})^2\left(1-S_{i-1}^{\frac{2+\lambda}{\lambda}}\right)}}{2(\Delta z)^2}S_{i-1}
\end{aligned}$$

Finally, the third term on the right-hand side contains the mixed derivatives of higher terms. We can approximate it in the same manner as we approximate the diffusion term, but now we also need to take into account the time derivative. The time derivatives will be approximated at two different time steps: t^n and t^{n+1} the following way:

$$\begin{aligned}
\frac{\partial}{\partial z}\left(M(S)\frac{\partial^2 S}{\partial z \partial t}\right)\Bigg|_i^n &\approx \frac{M\left(S^n_{i+\frac{1}{2}}\right)\frac{\partial^2 S}{\partial z\partial t}\big|^n_{i+\frac{1}{2}} - M\left(S^n_{i-\frac{1}{2}}\right)\frac{\partial^2 S}{\partial z\partial t}\big|^n_{i-\frac{1}{2}}}{\Delta z} \\
&\approx M\left(S^n_{i+\frac{1}{2}}\right)\left(\frac{S^{n+1}_{i+1}-S^{n+1}_i}{(\Delta z)^2\Delta t} - \frac{S^n_{i+1}-S^n_i}{(\Delta z)^2\Delta t}\right) \\
&\quad - M\left(S^n_{i-\frac{1}{2}}\right)\left(\frac{S^{n+1}_i - S^{n+1}_{i-1}}{(\Delta z)^2\Delta t} - \frac{S^n_i - S^n_{i-1}}{(\Delta z)^2\Delta t}\right) \\
&\approx \frac{M\left(S^n_{i+1}\right)+M\left(S^n_i\right)}{2}\left(\frac{S^{n+1}_{i+1}-S^{n+1}_i}{(\Delta z)^2\Delta t} - \frac{S^n_{i+1}-S^n_i}{(\Delta z)^2\Delta t}\right) \\
&\quad - \frac{M\left(S^n_i\right)+M\left(S^n_{i-1}\right)}{2}\left(\frac{S^{n+1}_i - S^{n+1}_{i-1}}{(\Delta z)^2\Delta t} - \frac{S^n_i - S^n_{i-1}}{(\Delta z)^2\Delta t}\right).
\end{aligned}$$

For the full discretization of the τ-term, we will follow the same procedure as we did for the diffusion term. Full application of IMEX method to the system of time dependent ODEs, gives rise to the system of equations in similar form as in (3.10).
The Table 3.1 contains the list of the parameter values, their symbols and units, used during numerical approximation of non equilibrium Richards' equation (2.20).

Parameter	**Symbol**	**Value**	**Units**
porosity	ϕ	0.35	[–]
conductivity	κ	0.0025	[m s^{-1}]
(total) flux	q	input	[m s^{-1}]
gravity acceleration	g	0.35	[m s^{-2}]
water density	ρ_w	998.21	[kg m^{-3}]
air density	ρ_o	1.2754	[kg m^{-3}]
water viscosity	μ_w	1.002 10^{-3}	[kg m^{-1} s^{-1}]
air viscosity	μ_o	1.82 10^{-5}	[kg m^{-1} s^{-1}]
mobility ratio	$M = \frac{\mu_w}{\mu_o}$	55.1	[–]
permeability	K	2.558 10^{-10}	[m^2]
effective water saturation	S		[–]
volumetric water saturation	θ	ϕS	[–]
residual saturation	θ_r	0.016	[–]
Brooks - Corey parameter	λ	5.5	[–]
entry pressure	h_d	8.66 10^{-2}	[m]
drainage	$P_d = \rho_w g h_d$	848	[kg m^{-1} s^{-2}]
imbibition	P_d	490	[kg m^{-1} s^{-2}]
diffusion coefficient	$d = \frac{p_w g h_d}{\lambda}$	152.25	[kg m^{-1} s^{-2}]
relative water permeability	K_{rw}	$S^{\frac{2+3\lambda}{\lambda}}$	[–]
relative air permeability	$K_{r\rho}$	$(S-1)^2\left(1 - S^{\frac{2+\lambda}{\lambda}}\right)$	[–]
water mobility	λ_w	$\frac{K}{\mu_w} K_{rw}$	[–]
air mobility	λ_o	$\frac{K}{\mu_o} K_{ro}$	[–]

Table 3.1: Parameter values, their symbols and units

Chapter 4

Analysis of traveling waves

Traveling waves represent particular type of solutions to PDE model (3.1) and (3.20). Essentially, we are assuming that a traveling wave solution has a certain form. We want to find the solution in the form $S(z,t) = \phi(z + ct)$, where c is wave velocity. Moving to traveling wave coordinates is an effective way to solve PDEs, because by using traveling wave transformation we can reduce given PDE to ODE, which is easier solvable.
When looking for a traveling wave solution we need to indicate which values (states) we want to connect. Therefore, we assume that we have a left value in the saturation, which is called left state (inflow state) and we also have a right state (initial state). We want to connect both states through the traveling wave that moves in time. This feature is shown in experiments of DiCarlo, where there is a sand column through which profile moves in time. When waiting long enough, except from the beginning, you will see that actually you get something like a wave moving constantly in time. Therefore the natural question that arises, is whether it is possible by means of mathematical analysis to reproduce an infiltration profile that moves constantly in time. Are the waves we receive monotonic or do they exhibit some overshoots or oscillations? These are all valid questions one can think of. Analysis of traveling wave solutions explains the occurrence of such type of phenomena. For the case when dynamic capillarity coefficient $\tau = 0$ the analysis is very straightforward. According to Evans [21], for viscous Burgers' equation, it is possible to compute the traveling waves explicitly for $c = 0$. Following the phase plane analysis, traveling wave solutions are possible if left state is larger than the right state, i.e $S_+ > S_-$. In this paper we are considering the case when $\tau > 0$ [1].

4.1 Phase plane analysis

To discuss the effect of different parameters on the saturation profile structure, we will apply the phase plane analysis technique to the PDE equation (3.1). We firstly introduce the traveling wave coordinate ξ, which is defined as:

$$\xi = z + ct.$$

Here, the constant c is the traveling wave speed and ξ is the traveling wave variable. Secondly, the traveling wave ansatz for velocity $S(x,t)$ reads:

$$S(z,t) = \phi(z+ct) = \phi(\xi),$$

where $\phi(\xi)$ is the wave profile and $\xi \in [-\infty, +\infty]$. Then

$$\frac{\partial}{\partial t} S(z,t) = c\frac{\partial}{\partial \xi}\phi(\xi) = c\phi', \tag{4.1}$$

$$\frac{\partial}{\partial t} S(z,t) = \frac{\partial}{\partial \xi}\phi(\xi) = \phi', \tag{4.2}$$

and

$$\frac{\partial}{\partial z^2} S(z,t) = \frac{\partial^2}{\partial \xi^2}\phi(\xi) = \phi''. \tag{4.3}$$

Substitution of (4.1), (4.2) and (4.3) into (3.1) yields:

$$c\frac{d}{\partial \xi}\phi(\xi) = d\frac{d^2}{\partial \xi^2}\phi(\xi) + \frac{d}{\partial \xi} f(\phi) + c\tau\frac{d}{\partial \xi}\left(\frac{d^2}{\partial \xi^2}\phi(\xi)\right), \tag{4.4}$$

or in simplified notation:

$$c\phi' = (d\phi')' + (f(\phi))' + c\tau(\phi'')'. \tag{4.5}$$

Equation (4.5) is written in traveling wave form and is completed with the following asymptotic boundary conditions:
$\phi(-\infty) = S_-, \qquad \phi(+\infty) = S_+, \qquad 0 < S_- < S_+ < 1,$
$\phi'(-\infty) = \phi'(+\infty) = 0, \qquad \phi''(-\infty) = \phi''(+\infty) = 0.$

Here S_- stands for the right boundary condition and S_+ stands for the left one. This implies that S_+ represents the saturation behind wetting the front (tail), while S_- is the saturation before the wetting front (tip).
We shall look for a steady profile moving with a constant velocity c, i.e. a traveling wave $S = \phi(\xi)$ as depicted in Figure 4.1.

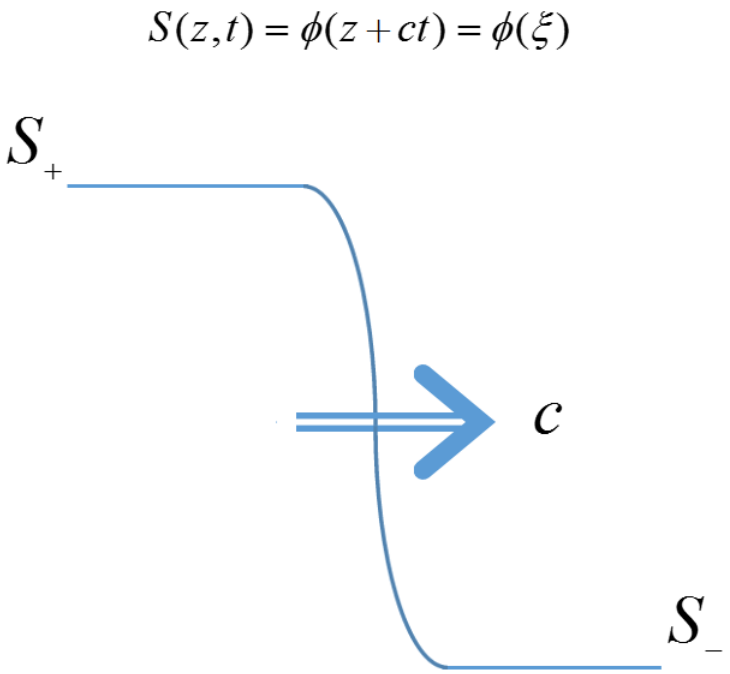

Figure 4.1: Sketch of a traveling wave with positive constant c

Here velocity c is given as:

$$c = \frac{f(S_+) - f(S_-)}{S_+ - S_-}.$$

Following [21], we integrate once the equation (4.4):

$$\begin{aligned}
&\int_{-\infty}^{\xi} \left(c\frac{d}{\partial\xi}\phi(\xi) \right) d\xi \\
&= \int_{-\infty}^{\xi} \left\{ d\frac{d^2}{\partial\xi^2}\phi(\xi) + \frac{d}{\partial\xi}f(\phi) + c\tau\frac{d}{\partial\xi}\left(\frac{d^2}{\partial\xi^2}\phi(\xi) \right) \right\} d\xi \\
&\Longleftrightarrow c\phi(\xi) - c\phi(-\infty) = d\frac{d}{\partial\xi}\phi(\xi) \\
&\Longleftrightarrow d\frac{d}{\partial\xi}\phi(-\infty) + f(\phi) - f(-\infty) + c\tau\frac{d^2}{\partial\xi^2}\phi(\xi) - c\tau\frac{d^2}{\partial\xi^2}\phi(-\infty)
\end{aligned}$$

Taking into account the boundary conditions of the traveling wave, gives us:

$$c\left(\phi(\xi) - S_-\right) = d\frac{d}{\partial\xi}\phi(\xi) + f(\phi) - f(S_-) + c\tau\frac{d^2}{\partial\xi^2}\phi(\xi). \tag{4.6}$$

Using a short notation, we can rewrite (4.6) as:

$$c(\phi - S_-) = d\phi' + f(\phi) - f(S_-) + c\tau\phi'',$$

which corresponds to a second order ordinary differential equation (ODE) and we can transform it into a system of two first order ODEs by introducing a new variable $\psi = \phi'$.
Then we have in the coordinates (ϕ, ψ):

$$\begin{cases} \phi' = \psi, \\ \psi' = \frac{c(\phi - S_-) - d\psi - f(\phi) + f(S_-)}{c\tau}. \end{cases} \tag{4.7}$$

If, for example, we assume that $f(S) = S^2$, we can rewrite (4.7) as:

$$\begin{cases} \phi' = \psi, \\ \psi' = \frac{c(\phi - S_-) - d\psi - \phi^2 + S^2}{c\tau}. \end{cases} \tag{4.8}$$

The system (4.8) has two stationary states, in other words two critical points, namely $(\phi, \psi) = (S_-, 0)$ and $(\phi, \psi) = (S_+, 0)$.
In order to specify the nature of the critical points, we firstly compute the Jacobian matrix of system (4.8) and then we determine its eigenvalues, which will allow us to investigate the type and stability of stationary states.

$$J = \begin{bmatrix} \frac{\partial \phi'}{\partial \phi} & \frac{\partial \phi'}{\partial \psi} \\ \frac{\partial \psi'}{\partial \phi} & \frac{\partial \psi'}{\partial \psi} \end{bmatrix} = \begin{bmatrix} 0 & 1 \\ \frac{c-2\phi'}{c\tau} & -\frac{d}{c\tau} \end{bmatrix}.$$

At the critical points the Jacobian matrix reads:

$$J = \begin{bmatrix} 0 & 1 \\ \frac{c-2u_{\pm}}{c\tau} & -\frac{d}{c\tau} \end{bmatrix}.$$

Applied to the critical points, we get:

$$J(S_-, 0) = \begin{bmatrix} 0 & 1 \\ \frac{c-2S_-}{c\tau} & -\frac{d}{c\tau} \end{bmatrix}.$$

Since $\det(J) = -\frac{c+2S_-}{c\tau} < 0$, it follows that critical point $(S_-, 0)$ is always a saddle point for all $\tau > 0$.
Next,

$$J(S_+, 0) = \begin{bmatrix} 0 & 1 \\ \frac{c-2S_+}{c\tau} & -\frac{d}{c\tau} \end{bmatrix}.$$

For point $(S_+, 0)$ we receive the following eigenvalues:

$$\lambda = -\frac{d}{2c\tau} \pm \sqrt{\frac{d^2}{4c^2\tau^2} + \frac{c-2S_+}{c\tau}}.$$

If, for example, we fix $S_- = 0$, $\tau = 3 \cdot 10^{-4}$ and $c = 0.6$, then at critical point $(S_+, 0)$ we obtain the following:

1. $d > d^* \approx 0.0041$
   In this case both eigenvalues are real and negative. This means that at critical point $(S_+, 0)$ we have a stable node. This case corresponds to weak damping i.e. monotonic decay.

2. $0 < d < d^* \approx 0.0041$
   In this case eigenvalues are complex conjugate with negative real part. Therefore at critical point $(S_+, 0)$ we have a stable focus. This case corresponds to strong damping or a so called oscillating front.

4.2 Numerical results

In this section we present the graphical representation of numerical solutions, which were obtained by applying the method of lines and IMEX integration scheme in approximation of the PDE model (3.1) from hydrology discussed in previous chapter. The chosen function $f(S) = S^2$, can be interpreted as fraction flow function, which has a convex-shaped profile. The initial condition (initial saturation) is given by the following function:

$$S(z,0) = S_- + \frac{1}{2}\left(S_+ - S_-\right)\left(1 + \tanh(R(z - z_0))\right), \tag{4.13}$$

with fixed parameter values: $S_- = 0$, $S_+ = 0.6$, $R = 50$ and $z_0 = 1.2$.
The graphical behavior of the numerical solutions is illustrated on the next pages in Figures 4.2 - 4.5, and can be explained by relating them to the traveling wave analysis we discussed in the previous section. Recall, that in the phase plane analysis we received only two critical points. This means that both states, S_+ and S_-, are connected directly through a traveling wave.
Throughout the whole simulation we change only the value of the diffusion (viscosity) coefficient d, while keeping fixed the non-equilibrium capillary coefficient τ, the right (S_-) and left (S_+) boundary values, the width of spatial and temporal time steps: $\tau = 3 \cdot 10^{-4}$, $S_- = 0$, $S_+ = 0.6$, $\Delta t = 0.001$ and $\Delta x = 0.01$. Figure 4.2 displays the non-monotone water saturation profile with many oscillations behind the wetting front corresponding to the case when the second critical point $(S_+, 0)$ represents focus in the phase plane. This means that the orbits spiral around the critical point, that is why we observe oscillations. Figures 4.3 and 4.4 show the non-monotone saturation profile with three and one oscillations, respectively. Here we consider the case when critical point $(S_+, 0)$ is a stable node. Figure 4.5 shows the monotonically decreasing saturation profile corresponding to the case when in the phase plane the orbits go directly to the second critical point $(S_+, 0)$, which is again a stable node.
The fractional flow function that we will use in the full model, for approximation of the DiCarlo infiltration experiments, has instead a convex-concaved profile. In terms of traveling wave analysis, this would mean that there will be three critical points. In other words, the traveling wave which connects left boundary value with the right one, goes through intermediate value [8]. This results in plateau-type saturation profiles. For detailed traveling wave analysis of convex-concave case, we are referring to [9, 23].

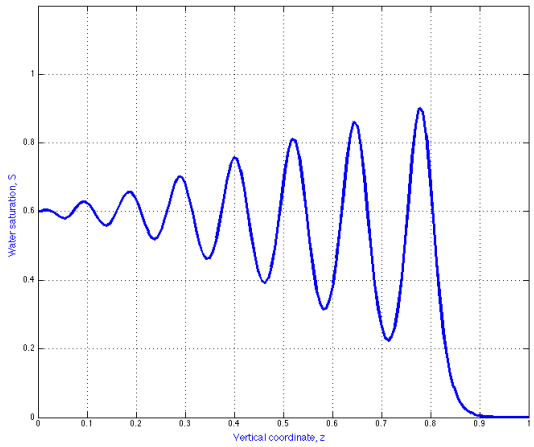

Figure 4.2: Non-monotone water saturation profile corresponding to the case when the second critical point is a stable focus in the phase plane. One phase flow with $\Delta x = 0.01$, $\Delta t = 0.001$, $\tau = 3 \cdot 10^{-4}$ and $d = 0.001$.

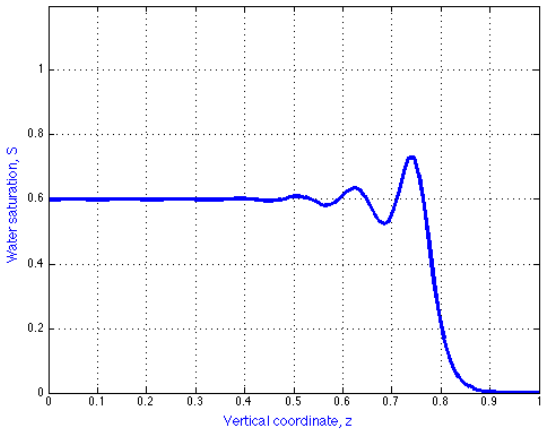

Figure 4.3: Non-monotone water saturation profile corresponding to the case when the second critical point is a stable node in the phase plane. One phase flow with $\Delta x = 0.01$, $\Delta t = 0.001$, $\tau = 3 \cdot 10^{-4}$ and $d = 0.005$.

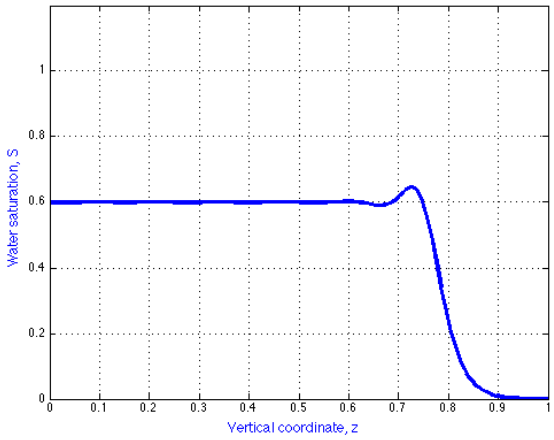

Figure 4.4: Non-monotone water saturation profile corresponding to the case when the second critical point is a stable node in the phase plane. One phase flow with $\Delta x = 0.01$, $\Delta t = 0.001$, $\tau = 3 \cdot 10^{-4}$ and $d = 0.01$.

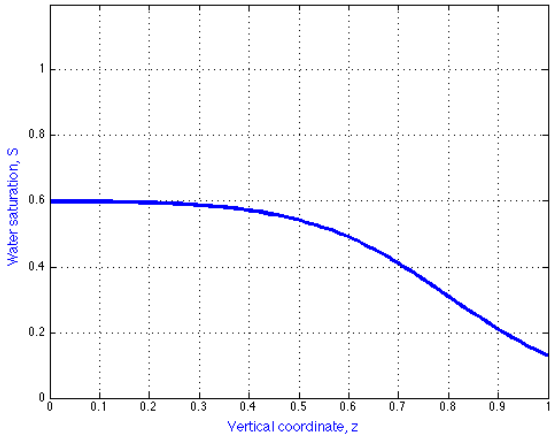

Figure 4.5: Monotone water saturation profile corresponding to the case when the second critical point is a stable node in the phase plane. One phase flow with $\Delta x = 0.01$, $\Delta t = 0.001$, $\tau = 3 \cdot 10^{-4}$ and $d = 0.1$.

Chapter 5

Numerical simulation vs experimental measurements

In this chapter, we present the results of several numerical experiments conducted for one-dimensional non-equilibrium two-phase flow model in porous media, both with and without inclusion of the hysteretic effects in calculation of capillary pressure function $P_c(S)$. All simulations were done on uniformly distributed fixed mesh.

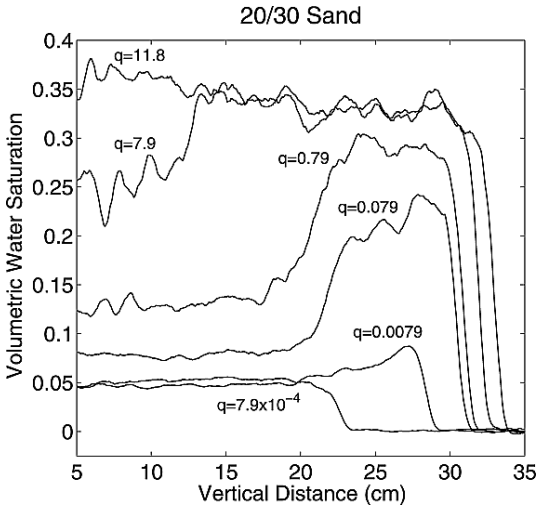

Plot	**DiCarlo injection rate** $q[\frac{cm}{min}]$	**Numercial injection rate** $q[\frac{m}{sec}]$
Plot 6	11.8	0.002
Plot 5	7.9	$1.32 \cdot 10^{-3}$
Plot 4	0.79	$1.32 \cdot 10^{-4}$
Plot 3	0.079	$1.32 \cdot 10^{-5}$
Plot 2	0.0079	$1.32 \cdot 10^{-6}$
Plot 1	$7.9 \cdot 10^{-4}$	$1.32 \cdot 10^{-7}$

Figure 5.1: (Left) Snapshot of the experimental measurements on infiltration performed by DiCarlo. (Right) Table summarizing the number of plots and their corresponding injection rates.

For the sake of clarity in Figure 5.1, we present the snapshot of six plots produced during DiCarlo's experiments, together with the summary of the injection rate values taken from experimental measurements and the corresponding values of injection rates used during numerical experiments. Note that DiCarlo in his experiments measures injection rates (q) in cm/min, while we use injection rates in m/s.
Recall that in chapter 4 we initially developed the numerical approximation scheme based on the method of lines (MOL) and IMEX integration technique assuming that flow in porous medium depends only on its saturation. Firstly we apply this scheme to approximate the non-equilibrium Richards' equation (2.11). Throughout the whole simulation we keep the damping parameter τ, the right boundary value S_-, the Brooks-Corey capillary pressure parameter P_d, the number of spatial and temporal grid points fixed, unless otherwise stated: $\tau = 30$, $S_- = 0.001$, $P_d = 850$, $I = 201$ and $N = 1201$.
The initial condition (initial saturation) is given by the following function:

$$S(z,0) = S_- + \frac{1}{2}\left(S_+ - S_-\right)\left(1 + \tanh(R(z - z_0))\right),$$

with fixed parameter values: $S_- = 0.001$, $R = 50$ and $z_0 = 0.1$.
Figure 5.2 illustrates the graphical results of numerical approximation corresponding to the six plots produced by DiCarlo at different values of the final time T.

Figure 5.2: Numerical simulation results of DiCarlo's experiments with method of lines in combination with IMEX.

Based on the experimental outcome, we can conclude that the method of lines in combination with IMEX works well. The monotone behavior depicted in plot 1 is almost identical in comparison with plot 1 from the original experiments of D. DiCarlo. The non-monotone saturation profile in plot 3 is consistent with the original experiments as well. In particular plot 4 clearly reproduces the desired infiltration overshoot in terms of the plateau type saturation profile.
Table 5.1 gives an overview of all variable parameters, which were used to produce the six plots illustrated in Figure 5.2. Here, for simplicity, the parameters are presented in dimensionless settings. The corresponding dimensions are listed in Table 3.1.

Parameter	**Plot 1**	**Plot 2**	**Plot 3**	**Plot 4**	**Plot 5**	**Plot 6**
τ	1500	1200	290	210	60	45
S_+	0.15	0.20	0.40	0.52	0.78	0.97
q	$1.32 \cdot 10^{-7}$	$1.32 \cdot 10^{-6}$	$1.32 \cdot 10^{-5}$	$1.32 \cdot 10^{-4}$	$1.32 \cdot 10^{-3}$	0.002
ε	0	0	0	0	$2 \cdot 10^{-6}$	$5 \cdot 10^{-6}$
λ	5.5	5.5	5.5	5.5	5.5	5.5

Table 5.1: Overview of parameters used by numerically approximate DiCarlo experiments.

Figure 5.3 shows the numerical approximation of plateau-type profile at incrementally decreasing values of temporal step sizes $\Delta t = 0.2, 0.1, 0.05, 0.025, 0.0125$ and 0.000625. It can be seen that profiles tend to overlap as Δt decreases, suggesting the convergence of numerical scheme.

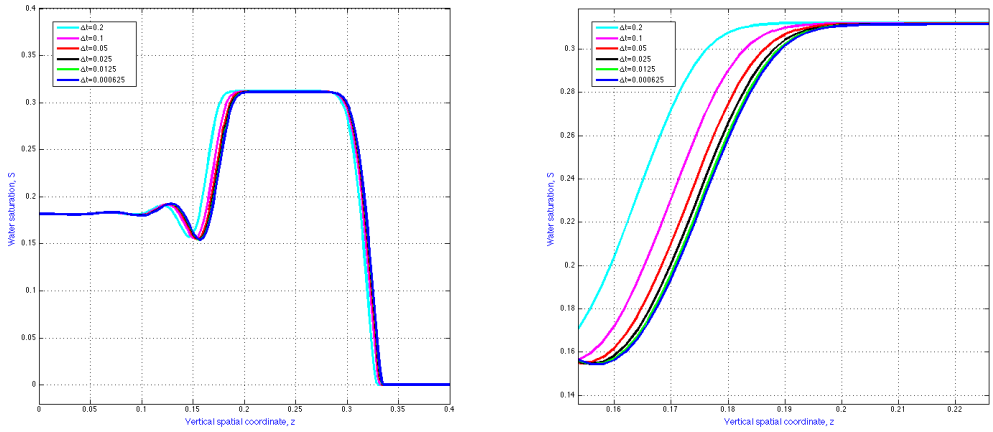

Figure 5.3: On the left the convergence of numerical approximation for plateau-type saturation profile (plot 4) at decreasing temporal step sizes $\Delta t = 0.2, 0.1, 0.05, 0.025, 0.00125$ and 0.000625. On the right the saturation profile (plot 4) zoom in at the region around the wetting front (tip).

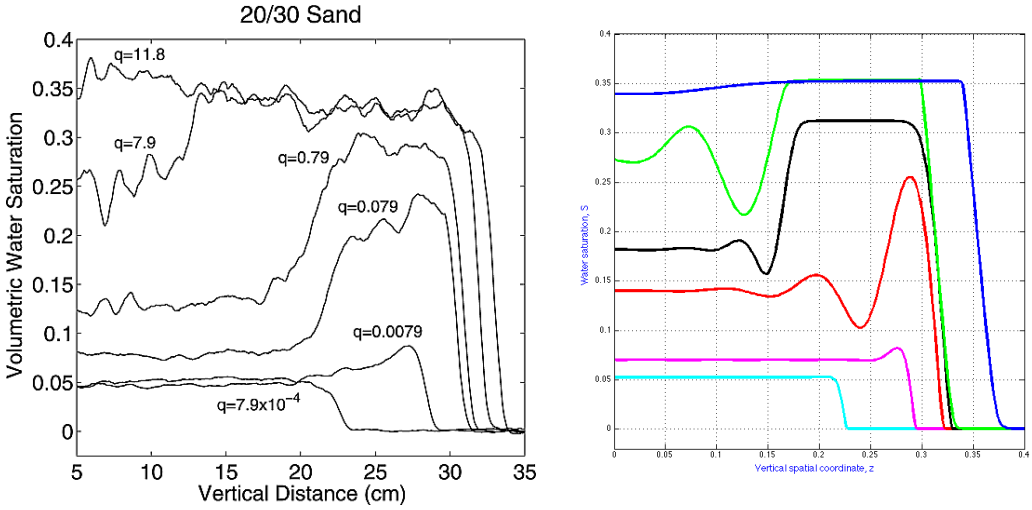

Figure 5.4: Experimental measurements of DiCarlo (left) versus numerical approximation (right).

Finally, in Figure 5.4 we combined all the plots to illustrate the comparison between the experimental measurements of DiCarlo versus the numerical simulation. As can be seen, the main shortcoming of the applied numerical scheme is the clear discrepancy between some of the left boundary values S_+ used to reproduce the experimental measurements numerically and those being used in original experiments. To allow for more accuracy of numerical solution, we extend in the next chapter the already existing numerical approximation scheme by introducing the effects of hysteresis in calculation of capillary pressure function $P_c(S)$. In other words, we are taking into consideration that fluid flow in porous media does not only depend on its saturation, but also has memory of flow displacements, i.e. the switch between imbibition and drainage phases.

Chapter 6

Hysteresis, drainage and imbibition

6.1 Overview

In chapter 5, we have seen that numerical approximation technique MOL in combination with Euler-Forward and Euler-Backward can produce convergent approximation of 1D vertical infiltration experiments performed by DiCarlo. The numerical results are particularly accurate for saturation profiles at sufficiently low water injection rates in porous media. The main shortcoming of obtained results, is obvious inconsistency between some of the left boundary values S_+ (left states) used to reproduce DiCarlo's experiments numerically and those being used in the original experiments by DiCarlo. In particular, we can observe that for saturation profiles which demonstrate monotonic behavior at the lower flux values, i.e. $q = 7.9 \cdot 10^{-4}[cm/min]$ and $q = 0.0079[cm/min]$ and the highest flux rate at $q = 11.8[cm/min]$, the mismatch at the left boundary values is small. However, at intermediate fluxes, such as $q = 0.079[cm/min]$ and $q = 0.79[cm/min]$ where we obtain saturation profiles exhibiting non-monotonic behavior, we observe significant divergence between the values at the left boundary used to produce the profiles numerically versus those profiles produced experimentally.

Figure 6.1 gives the clear illustration of what happens with the graphical image if we apply the numerical approximation scheme to the fourth plot (Figure 5.1), using the left boundary value which fits our numerical experiments, $S_+ = 0.52$, versus the numerical approximation scheme with the original left boundary value used by DiCarlo, $S_+ = 0.34$, given that all other parameters are equal. As left boundary value (left state) S_+ decays, the plateau-type saturation profile vanishes and the approximated solution transforms into an oscillatory front.

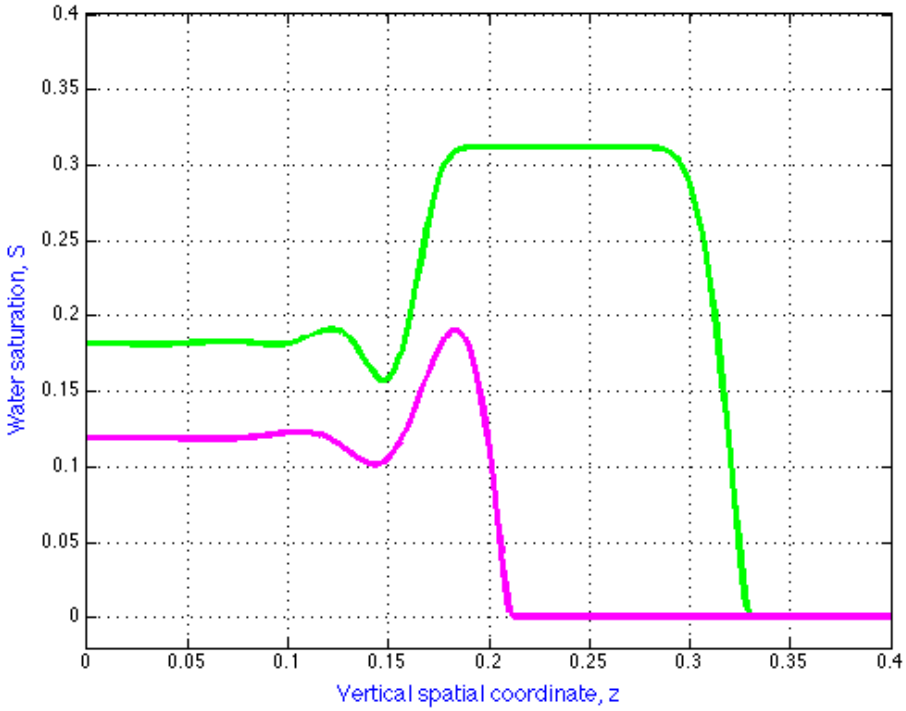

Figure 6.1: The green line shows the numerical solution using the left boundary value which fits our numerical experiments $S_+ = 0.52$. The pink line shows the numerical solution using the left boundary value $S_+ = 0.34$, which is taken from experimental measurements performed by DiCarlo.

In the next table, we summarize the above-mentioned results by specifying the exact values taken at the left boundary for six plots produced originally by DiCarlo versus the corresponding six plots produced by the numerical approximation scheme (from lowest to the highest injection rate).

Plot	**Left boundary values S_+ in experiments of DiCarlo**	**Left boundary value S_+ in numerical approximation scheme**	**Difference between numerical S_+ and original S_+**	**DiCarlo injection rate $q[\frac{cm}{min}]$**
Plot 1	0.12	0.15	0.03	$7.9 \cdot 10^{-4}$
Plot 2	0.12	0.20	0.08	0.0079
Plot 3	0.23	0.40	0.17	0.079
Plot 4	0.34	0.52	0.18	0.79
Plot 5	0.74	0.78	0.04	7.9
Plot 6	0.97	0.97	0	11.8

Table 6.1: Comparison between left boundary values used in the constant flux infiltration experiments of DiCarlo versus left boundary values used to re-produce experiments of DiCarlo numerically.

One of the reasons, why we observe these discrepancies at the left boundary is because up till now we neglected so called hysteretic effects in modeling of capillary pressure function. Numerically approximating the two-phase flow model in porous media, so far, we only considered the influence of dynamic effects on the saturation profiles. In this chapter, we will discuss the notion of imbibition and drainage and we will extend the results obtained previously by including the effects of hysteresis to already existing model.

6.2 Measurement of capillary pressure

In this section we are presenting a summary on the measurement of capillary pressure-saturation curves in laboratory conditions from [6], [9] and [10].
The soil sample is placed in the pressure plate apparatus, which contains two reservoirs: non-wetting reservoir and wetting reservoir. These reservoirs contact with the soil sample. Initially if two pressures are equal and one of the reservoirs is filled with wetting phase (water) nothing will happen because it is in equilibrium modus. Therefore we can plot pressure difference

curve $p_o - p_w = P_c(S)$. In this way, the first point is obtained. The process is repeated, by increasing the pressure incrementally and so forth. Nothing will happen until the threshold value is surpassed. At this point some water goes out and some non-wetting phase gets in. Only after the equilibrium is reached again (i.e. there is no any movement of phases at all), another measurement can be done. By plotting again the new pressure difference against the saturation, another point is obtained. This measurement process is repeated several times and in the end we get a drying curve or so called drainage curve. We can now reverse the process, either by putting water back in by increasing water pressure or reducing the non-wetting phase pressure. However, we do not get the same curve. Instead we get a different curve. Here data points fell on the different curve, which is significantly different. And this is called the wetting curve or so called imbibition curve. If the reversal of phases happens on the half way from drying curve to wetting curve and vice versa, we get other curves, so called scanning curves: scanning wetting curve or scanning drying curve. Therefore there is not just a single curve. Moreover, not the actual pressures are measured inside but the pressure outside of the soil sample is measured. In order to get the set of above-mentioned curves sometimes it can take more than a week. Here we are considering that very slow processes are taking place. The static algebraic relationship of capillary pressure holds only if the equilibrium is reached. But very often the same curves, which were obtained in static experiments, as described above, are used for processes that are taking place much faster.

In the past, experiments were performed to see what happens if measurements of pressure inside soil are made as the process occur, meaning without reaching equilibrium state. In these kinds of experiments, pressure transducers are added: hydrophobic and hydrophilic. One measures water pressure and the other one measures air (oil) pressure. The measurements of the pressure were performed as the flow occurred. These kinds of experiment are dynamic experiments. It means pressure is increased to a large value and the processes within the experiment occur very quickly. The pressure difference curves that were obtained during the dynamic experiment, compared to those obtained in static experiments, were significantly different.

These experiments proved that standard theory does not model non-monotonic distribution of saturation during the infiltration as well as that capillary pressure function $P_c(S)$ is not presented only by one curve.

6.3 Hysteresis

The notion of the hysteresis mode emerges as the result of flow displacement between two phases: wetting (imbibition) and non-wetting (drainage). Recall, that per definition imbibition occurs when a wetting fluid displaces a non-wetting fluid, i.e. the wetting-phase saturation is increasing. Oppositely, drainage occurs when non-wetting phase displaces a wetting fluid, i.e. if wetting-phase saturation is decreasing. Therefore hysteresis is the process that keeps track of type and number of reversal events (from drainage to imbibition or vice versa), which occur in the different saturation directions [13].

In this section we extend the already developed numerical approximation scheme described in detail in chapter 3, by assuming that capillary pressure function $P_c(S)$, which describes the relationship of saturation and capillary pressure, has memory for previous events. In order to include hysteretic effects in our numerical approximation scheme, we follow the procedure as pointed in [2], [14], [15] and [18]. As before, we assume a 1D fluid flow.

Based on equation (3.20), the corresponding mathematical model for non-equilibrium hysteretic two-phase flow (air-water) in porous medium can be written down as:

$$\begin{aligned}\phi\frac{\partial S}{\partial t}+\Omega(S)\frac{\partial}{\partial z}\left[g_{im}(S)-D_{im}(S)\frac{\partial S}{\partial z}-\tau M_{im}(S)\frac{\partial^2 S}{\partial z\partial t}\right]+\\ \left[1-\Omega(S)\right]\frac{\partial}{\partial z}\left[g_{dr}(S)-D_{dr}(S)\frac{\partial S}{\partial z}-\tau M_{dr}(S)\frac{\partial^2 S}{\partial z\partial t}\right]=0,\end{aligned} \tag{6.1}$$

where left side limit $\Omega(S)$ can be expressed as:

$$\Omega(S)=\lim_{\eta\to 0}\Phi\left(\frac{\partial S}{\partial t}(z,t-\eta)\right), \tag{6.2}$$

with the Heaviside step function $\Phi(S)$ satisfying the following condition relation:

$$\Phi(S)=\begin{cases}1, & \text{if } \frac{\partial S}{\partial t}>0\\ 0, & \text{if } \frac{\partial S}{\partial t}\leq 0\end{cases}.$$

From the two commonly used approaches known in literature as models of Brooks-Corey and Van Genuchten, used to relate relative permeability to saturation, we are going to use Brooks-Corey type relative permeability for each phase [20]:

$$k_{rwi} = S_i^{\frac{2+3\lambda_i}{\lambda_i}}, \tag{6.3}$$

$$k_{rai} = (1 - S_i)^2(1 - S^{\frac{2+\lambda_i}{\lambda_i}}), \tag{6.4}$$

where k_{rw} and k_{ra} stand for relative water and air permeabilities respectively. Index $i \in \{im, dr\}$.
Previously, disregarding the hysteretic effects from the calculation of the capillary pressure function $P_c(S)$, we kept Brooks-Corey parameters $\lambda = 5.5$ and $P_d = 850[kgm^{-1}s^{-1}]$ fixed throughout the whole computation, explicitly assuming that we are always in drainage phase, i.e. $\frac{\partial S}{\partial t} \leq 0$.

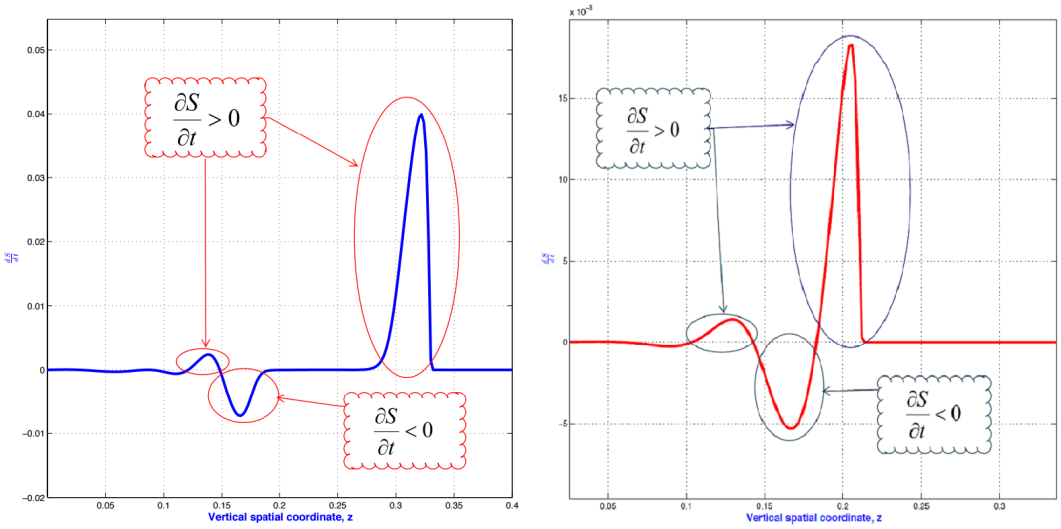

Figure 6.2: Figure graphically illustrates two Brooks-Corey type capillary pressure curves: the red curve corresponds to drainage case, while the blue one corresponds to imbibition case.

Figure 6.2 shows the snapshots of two $\frac{\partial S}{\partial t}$ curves, corresponding to the fourth plot of numerical approximation solution from chapter 3, with left boundary value $S_+ = 0.52$ on the left and $S_+ = 0.34$ on the right. What we can obviously see, is that $\frac{\partial S}{\partial t}$ curves in both figures do not necessarily always take negative or equal to 0 values. At some points in space direction, $\frac{\partial S}{\partial t}$ curves also take positive values, i.e. $\frac{\partial S}{\partial t} > 0$. Therefore, our initial assumption that capillary pressure function always corresponds to non-wetting phase, was false.

As the result, approximating the mathematical model (6.1), we need now to consider the two situations:

$$\begin{cases} \frac{\partial S}{\partial t} \leq 0 & \Rightarrow \text{drainage phase, } \lambda = 5.5 \text{ and } P_d = 850 \\ \frac{\partial S}{\partial t} > 0 & \Rightarrow \text{imbibition phase, } \lambda = 5 \text{ and } P_d = 490 \end{cases}.$$

Finally, the expression describing hysteretic capillary pressure function $P_c(S)$ reads as follows:

$$P_{ci}(S) = P_{di} S^{-\frac{1}{\lambda_i}} \Rightarrow \left| P_{ci}^{'} \right| = \frac{P_{di}}{\lambda_i} S^{\frac{\lambda_i + 1}{\lambda_i}}. \tag{6.5}$$

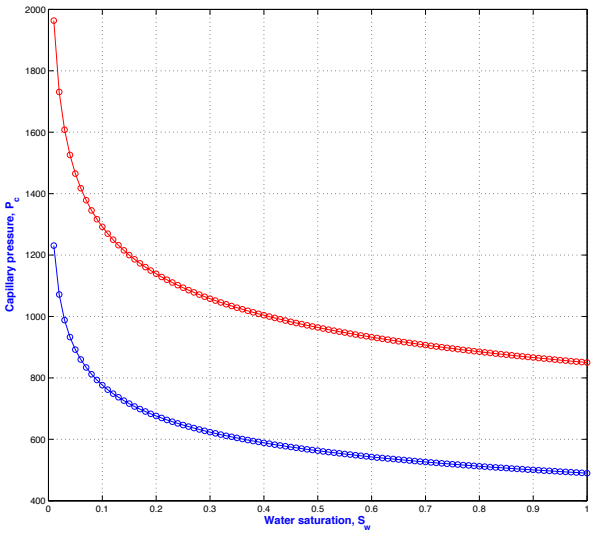

Figure 6.3: The blue line corresponds to Brooks-Corey imbibition curve for case $P_d = 490$ and $\lambda = 5$. The red line corresponds to Brooks-Corey drainage curve for case $P_d = 850$ and $\lambda = 5.5$

6.4 Numerical results

We are going to focus our attention only on the numerical improvement of the fourth plot with the injection rate $q = 0.79$ (Figure 5.4), as it has the biggest inconsistency at the left boundary value from all of the six results. Figure 6.4 shows the difference between the implementation of the numerical scheme, which takes into account only the dynamic capillary pressure effects versus the numerical scheme, which considers dynamic capillary pressure effects as well as hysteretic effects.

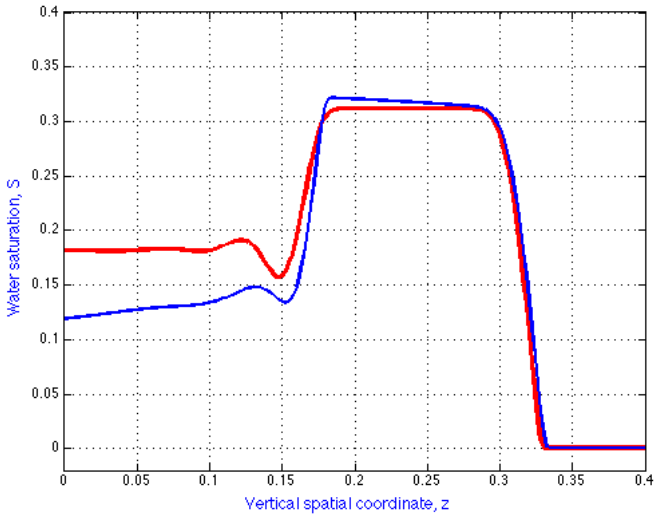

Figure 6.4: The red curve corresponds to numerical solution of plateau type saturation profile (plot 4) excluding hysteretic effects. The blue curve corresponds to numerical solution of plateau type saturation profile (plot 4) including hysteretic effects.

The plot clearly demonstrates the advantage of including the switch between the wetting and the non-wetting phases in the numerical simulation, as now it is able to produce a plateau type solution with original value at the left boundary condition.
Again, we check the convergence of enhanced numerical scheme by incrementally decreasing values of temporal step sizes $\Delta t = 0.2, 0.1, 0.05, 0.025, 0.0125$ and 0.000625 while keeping the value of Δz fixed: $\Delta z = 0.0020$. The results

depicted in Figure 6.5 acknowledges the convergence of numerical approximation method.

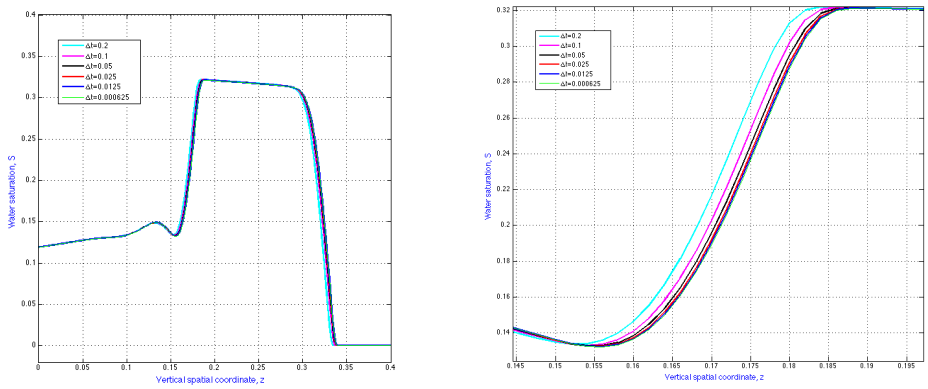

Figure 6.5: (left) The convergence of numerical approximation scheme including hysteretic effects for plateau-type saturation profile (plot 4) at temporal step sizes $\Delta t = 0.2, 0.1, 0.05, 0.025, 0.00125$ and 0.000625. (right) The saturation profile (plot 4) zoom in at the region around the wetting front (tip).

Chapter 7

Conclusion

The main focus of this thesis was to reproduce, by means of advanced numerical techniques, the experimental measurements of saturation overshoot during infiltration that occur in the flow in porous media, as described by DiCarlo. This was of the particular interest as such dynamic phenomenon as saturation overshoots are not treated by standard mathematical models that are conventionally used to describe flow in porous medium. Throughout this paper, the theory of traveling wave analysis was tightly integrated with the solutions of numerical approximation of the governing equation.
In this paper, we initially developed the non-equilibrium model with high-order mixed derivative term for two phase flow (air-water) in porous media, which accounted for the dynamic effects in the capillary pressure function, to which we successfully applied the numerical approximation scheme based on Method of Lines (MOL) in combination with an IMEX time integration scheme. The outcome of the numerical result was highly influenced by the chosen values, therefore the importance of specific choice of the constant parameters and functions suitable for experiments was outlined throughout the whole research. The effect of the damping parameter τ still needs more profound investigation.
In summary, the chosen numerical approach produced a relatively accurate numerical solution, while the graphical visualization indicated the convergence of the numerical scheme. The obvious shortcoming of the numerical approximation at the left boundary values, was improved by including the effects of hysteresis to the already existing model.

Appendix A

Matlab Code

```
%-------------------------------------------------------------------%
% Definition of parameters
%-------------------------------------------------------------------%
% number of spatial grid points
I=201;
% number of temporal grid points
N=1201;
% non-equilibrium capillarity coefficient
tau=30;
% injection rate
q=1.32*10^-4;
% left boundary value
ub=0.52;
% final time
T=210;
% artificial parameter
epsilon=0;
% right boundary value
ua=0.001;
% porosity
poros=0.35;
L=0.4;
% width of each space step
dx=L/(I-1);
% width of each time step
```

```
dt= T/(N-1);
x0=0.1;
% entry pressure
h_d = 8.66*10^-2;
% Brooks-Corey parameter
lambda=5.5;
mu=850/lambda;
% water viscosity
mu_w=1.002*10^-3;
% air viscosity
mu_o=1.82*10^-5;
% mobility ratio
A=mu_w/mu_o;
u_old(1,:)=ub;
u_old(I,:)=ua;
% derivative of water saturation
ds_dt(:,:)=zeros;
% preallocation of variable for faster speed of
    calculation
u_new(N,:)=zeros;
% preallocation of variable for faster speed of
    calculation
x(I,:)=zeros;
% definition of relative air permeability
k_ro(I,:)=zeros;
% definition of air mobility
lambda_o(I,:)=zeros;
% definition of fractional flow function
f(I,:)=zeros;
% denition of the first element of vector g
g(1,:)=0;
% denition of the last element of vector g
g(I,:)=0;
% preallocation of variable for faster speed of
    calculation
g(I,:)=zeros;
% permeability
K=2.558*10^-10;
```

```
% gravitational acceleration
g_accel=9.81;
% water density
ro_w=998.21;
% air density
ro_o=1.2754;
% difference between water and air densities
delta_ro=ro_w-ro_o;
% definition of matrix D
D = zeros(I);
% definition of matrix M
M = zeros(I);
% definition of the first element of matrix M
M(1,1)=1;
% definition of the last element of matrix M
M(I,I)=1;

%-------------------------------------------------------------------%
% Calculation of spation grid point x(i)
%-------------------------------------------------------------------%
for i = 1:I
    x(i)= (i-1)*L/(I-1);
end %for i = 1:I

%-------------------------------------------------------------------%
% Calculation of initial condition u_old
%  at each grid point i
%-------------------------------------------------------------------%
for i = 2:I-1
    u_old(i)= ua + 0.5*(ub-ua)*(1-tanh(50*(x(i)-x0)));
end %for i = 2:I-1

%-------------------------------------------------------------------%
% First step of method of lines
% (discretization of spatial derivatives only)
%-------------------------------------------------------------------%
for i= 2:I-1
```

```
M(i,i-1)= -tau*((((K/mu_o)*(1-u_old(i))^2*(1-u_old(i)
    ^((2+lambda)/lambda))*(u_old(i)^((2+3*lambda)/lambda
    ))*...
abs(mu*(u_old(i)^(-(lambda+1)/lambda))))/(  u_old(i)
    ^((2+3*lambda)/lambda)+...
A*(1-u_old(i))^2*(1-u_old(i)^((2+lambda)/lambda))))/(2*
    dx^2)+(((K/mu_o)*(1-u_old(i-1))^2*(1-u_old(i-1)^((2+
    lambda)/lambda))*...
(u_old(i-1)^((2+3*lambda)/lambda))...
*abs( mu*(u_old(i-1)^(-(lambda+1)/lambda))))/(u_old(i
    -1)^((2+3*lambda)/lambda)+A*(1-u_old(i-1))^2*(1-
    u_old(i-1)^((2+lambda)/lambda))))...
/(2*dx^2));
M(i,i)= (poros+tau*((((K/mu_o)*(1-u_old(i+1))^2*(1-
    u_old(i+1)^ ((2+lambda) /lambda))*(u_old(i+1)^((2+3*
    lambda)/lambda))...
*abs( mu*(u_old(i+1)^(-(lambda+1)/lambda))))/(  u_old(i
    +1)^((2+3*lambda)/lambda)+...
A*(1-u_old(i+1))^2*(1-u_old(i+1)^((2+lambda)/lambda))))
    /(2*dx^2)+  (((K/mu_o)*(1-u_old(i))^2*(1-u_old(i)
    ^((2+lambda)/lambda))...
*(u_old(i)^((2+3*lambda)/lambda))*abs(mu*(u_old(i)^(-(
    lambda+1)/lambda))))/(  u_old(i)^((2+3*lambda)/lambda
    )+...
A*(1-u_old(i))^2*(1-u_old(i)^((2+lambda)/lambda))))/(dx
    ^2)+(((K/mu_o)*(1-u_old(i-1))^2*(1-u_old(i-1)^((2+
    lambda)/lambda))...
*(u_old(i-1)^((2+3*lambda)/lambda))*abs( mu*(u_old(i-1)
    ^(-(lambda+1)/lambda))))/(u_old(i-1)^((2+3*lambda)/
    lambda)+...
A*(1-u_old(i-1))^2*(1-u_old(i-1)^((2+lambda)/lambda))))
    /(2*dx^2)));
M(i,i+1)= -tau*((((K/mu_o)*(1-u_old(i))^2*(1-u_old(i)
    ^((2+lambda)/lambda))*(u_old(i)^((2+3*lambda)/lambda
    ))*...
abs( mu*(u_old(i)^(-(lambda+1)/lambda))))/(  u_old(i)
    ^((2+3*lambda)/lambda)+...
```

```
A*(1-u_old(i))^2*(1-u_old(i)^((2+lambda)/lambda)))/(2*
    dx^2)+(((K/mu_o)*(1-u_old(i+1))^2*(1-u_old(i+1)^((2+
    lambda) /lambda))*...
(u_old(i+1)^((2+3*lambda)/lambda))*abs( mu*(u_old(i+1)
    ^(-(lambda+1)/lambda))))/(u_old(i+1)^((2+3*lambda)/
    lambda)+A*(1-u_old(i+1))^2*...
(1-u_old(i+1)^((2+lambda)/lambda))))/(2*dx^2));
end % for i= 2:I-1

%-------------------------------------------------------------------%
% Discretization of matrix D in space
% (time is continuous)
%-------------------------------------------------------------------%
for i= 2:I-1
D(i,i-1)= (((K/mu_o)*(1-u_old(i))^2*(1-u_old(i)^((2+
    lambda)/lambda))*(u_old(i)^((2+3*lambda)/lambda))
    *...
abs(mu*(u_old(i)^(-(lambda+1)/lambda))))/( u_old(i)
    ^((2+3*lambda)/lambda)+...
A*(1-u_old(i))^2*(1-u_old(i)^((2+lambda)/lambda)))+
    epsilon)/(2*dx^2)+(((K/mu_o)*...
(1-u_old(i-1))^2*(1-u_old(i-1)^((2+lambda)/lambda))*(
    u_old(i-1)^((2+3*lambda)/lambda))*...
abs(mu*(u_old(i-1)^(-(lambda+1)/lambda))))/(u_old(i-1)
    ^((2+3*lambda)/lambda)+A*(1-u_old(i-1))^2*...
(1-u_old(i-1)^((2+lambda)/lambda))) +epsilon)/(2*dx^2);
D(i,i)= -((((K/mu_o)*(1-u_old(i+1))^2*(1-u_old(i+1)^
    ((2+lambda) /lambda))*(u_old(i+1)^((2+3*lambda)/
    lambda))*...
abs( mu*(u_old(i+1)^(-(lambda+1)/lambda))))/( u_old(i
    +1)^((2+3*lambda)/lambda)+ A*(1-u_old(i+1))^2*...
(1-u_old(i+1)^((2+lambda)/lambda)))+epsilon)/(2*dx^2)+
    (((K/mu_o)*(1-u_old(i))^2*(1-u_old(i)^((2+lambda)/
    lambda))*...
(u_old(i)^((2+3*lambda)/lambda))*abs(mu*(u_old(i)^(-(
    lambda+1)/lambda))))/( u_old(i)^((2+3*lambda)/lambda
    )+ A*(1-u_old(i))^2*...
```

```
(1-u_old(i)^((2+lambda)/lambda)))+epsilon)/(dx^2)+(((K/
    mu_o)*(1-u_old(i-1))^2*(1-u_old(i-1)^((2+lambda)/
    lambda))*...
(u_old(i-1)^((2+3*lambda)/lambda))*abs( mu*(u_old(i-1)
    ^(-(lambda+1)/lambda))))/(u_old(i-1)^((2+3*lambda)/
    lambda)+ A*(1-u_old(i-1))^2*...
(1-u_old(i-1)^((2+lambda)/lambda)))+epsilon)/(2*dx^2));
D(i,i+1)=(((K/mu_o)*(1-u_old(i))^2*(1-u_old(i)^((2+
    lambda)/lambda))*(u_old(i)^((2+3*lambda)/lambda))
    *...
abs( mu*(u_old(i)^(-(lambda+1)/lambda))))/( u_old(i)
    ^((2+3*lambda)/lambda)+ A*...
(1-u_old(i))^2*(1-u_old(i)^((2+lambda)/lambda)))+
    epsilon)/(2*dx^2)+(((K/mu_o)*(1-u_old(i+1))^2*(1-
    u_old(i+1)^((2+lambda)/lambda))...
*(u_old(i+1)^((2+3*lambda)/lambda))*abs( mu*(u_old(i+1)
    ^(-(lambda+1)/lambda))))/(u_old(i+1)^((2+3*lambda)/
    lambda)+A*(1-u_old(i+1))^2*...
(1-u_old(i+1)^((2+lambda)/lambda)))+epsilon)/(2*dx^2);
end % for i= 2:I-1

%-------------------------------------------------------------------%
% Discretization of fractional flow function in space
% (time is continuous)
%-------------------------------------------------------------------%
for i = 2:I-1

a= q*((u_old(i+1)^((2+3*lambda)/lambda))/(u_old(i+1)
    ^((2+3*lambda)/lambda)+A*(1-u_old(i+1))^2*(1-u_old(i
    +1)^((2+lambda)/lambda))))...
+g_accel*delta_ro*(((K/mu_o)*(1-u_old(i+1))^2*(1-u_old(
    i+1)^((2+lambda)/lambda))*...
(u_old(i+1)^((2+3*lambda)/lambda)))/(u_old(i+1)^((2+3*
    lambda)/lambda)+ A*(1-u_old(i+1))^2*(1-u_old(i+1)
    ^((2+lambda)/lambda))));

b= q*((u_old(i-1)^((2+3*lambda)/lambda))/(u_old(i-1)
    ^((2+3*lambda)/lambda)+A*(1-u_old(i-1))^2*(1-u_old(i
```

```
    -1)^((2+lambda)/lambda))))+...
g_accel*delta_ro*(((K/mu_o)*(1-u_old(i-1))^2*(1-u_old(i
    -1)^((2+lambda)/lambda))*(u_old(i-1)^((2+3*lambda)/
    lambda)))/...
(u_old(i-1)^((2+3*lambda)/lambda)+ A*(1-u_old(i-1))
    ^2*(1-u_old(i-1)^((2+lambda)/lambda))));

% Central finite difference scheme
g(i)= -((a-b)/(2*dx));
end % for i = 2:I-1

%-------------------------------------------------------------------%
% Second step of MOL (approximation in time)
%  Initialization of u
%-------------------------------------------------------------------%
u=u_old;

%-------------------------------------------------------------------%
% Implementation IMEX method
%  (Euler Forward-Euler Backward scheme)
%-------------------------------------------------------------------%
for n=1:N

%  Calculation of saturation vector u at every time
    step
        u_new=(M-dt*D)\(M*u+dt*g);
%  Calculation of saturation derivative
        ds_dt=(u_new-u)/dt;
        u=u_new;

%-------------------------------------------------------------------%
% Approximation of fractional flow function
%  in space and time
%-------------------------------------------------------------------%
for i = 2:I-1
c= q*((u(i+1)^((2+3*lambda)/lambda))/(u(i+1)^((2+3*
    lambda)/lambda)+A*(1-u(i+1))^2*(1-u (i+1)^((2+lambda
    )/lambda))))+g_accel*delta_ro...
```

```
*(((K/mu_o)*(1-u(i+1))^2*(1-u (i+1)^((2+lambda)/lambda)
    )*(u (i+1)^((2+3*lambda)/lambda)))/(u(i+1)^((2+3*
    lambda)/lambda)+...
A*(1-u(i+1))^2*(1-u(i+1)^((2+lambda)/lambda))));

d= q*((u(i-1)^((2+3*lambda)/lambda))/(u(i-1)^((2+3*
    lambda)/lambda)+A*(1-u(i-1))^2*(1-u(i-1)^((2+lambda)
    /lambda)))) ...
+g_accel*delta_ro*(((K/mu_o)*(1-u(i-1))^2*(1-u (i-1)
    ^((2+lambda)/lambda))*...
(u(i-1)^((2+3*lambda)/lambda)))/(u(i-1)^((2+3*lambda)/
    lambda) ...
+ A*(1-u(i-1))^2*(1-u(i-1)^((2+lambda)/lambda))));

% Central finite difference scheme
g(i)= -((c-d)/(2*dx));

%Approximation of matrix M in space and time
% (second step in MOL)
M(i,i-1)= -tau*((((K/mu_o)*(1-u(i))^2*(1-u(i)^((2+
    lambda)/lambda))*(u(i)^((2+3*lambda)/lambda))*...
abs(mu*(u(i)^(-(lambda+1)/lambda))))/( u(i)^((2+3*
    lambda)/lambda)+...
A*(1-u(i))^2*(1-u(i)^((2+lambda)/lambda))))/(2*dx^2)
    +(((K/mu_o)*(1-u(i-1))^2*(1-u(i-1)^((2+lambda)/
    lambda))*...
(u(i-1)^((2+3*lambda)/lambda))*abs( mu*(u(i-1)^(-(
    lambda+1)/lambda))))/(u(i-1)^((2+3*lambda)/lambda)+A
    *(1-u(i-1))^2*...
(1-u(i-1)^((2+lambda)/lambda))))/(2*dx^2));

M(i,i)= (poros+tau*((((K/mu_o)*(1-u(i+1))^2*(1-u(i+1)
    ^((2+lambda)/lambda))*(u(i+1)^((2+3*lambda)/lambda))
    *...
abs( mu*(u(i+1)^(-(lambda+1)/lambda))))/(u(i+1)^((2+3*
    lambda)/lambda)+ A*(1-u(i+1))^2*...
(1-u(i+1)^((2+lambda)/lambda))))/(2*dx^2)+(((K/mu_o)
    *(1-u(i))^2*(1-u(i)^((2+lambda)/lambda))*(u(i)
```

```
    ^((2+3*lambda)/lambda)) ...
*abs(mu*(u(i)^(-(lambda+1)/lambda))))/(u(i)^((2+3*
    lambda)/lambda)+A*(1-u(i))^2*(1-u(i)^((2+lambda)/
    lambda))))/(dx^2)+(((K/mu_o) ...
*(1-u(i-1))^2*(1-u(i-1)^((2+lambda)/lambda))*(u(i-1)
    ^((2+3*lambda)/lambda)) *...
abs( mu*(u(i-1)^(-(lambda+1)/lambda))))/(u(i-1)^((2+3*
    lambda)/lambda)+ A*(1-u(i-1))^2*(1-u(i-1)^((2+lambda
    )/lambda))))/(2*dx^2)));

M(i,i+1)=-tau*((((K/mu_o)*(1-u(i))^2*(1-u(i)^((2+lambda
    )/lambda))*(u(i)^((2+3*lambda)/lambda)) ...
*abs( mu*(u(i)^(-(lambda+1)/lambda))))/(u(i)^((2+3*
    lambda)/lambda)+ A*(1-u(i))^2*(1-u(i)^((2+lambda)/
    lambda))))/(2*dx^2) ...
+(((K/mu_o)*(1-u(i+1))^2*(1-u(i+1)^((2+lambda) /lambda)
    )*(u(i+1)^((2+3*lambda)/lambda)) *...
abs( mu*(u(i+1)^(-(lambda+1)/lambda))))/(u(i+1)^((2+3*
    lambda)/lambda)+A*(1-u(i+1))^2*(1-u(i+1)^((2+lambda)
    /lambda))))/(2*dx^2));

%Approximation of matrix M in space and time
% (second step in MOL)
D(i,i-1)= (((K/mu_o)*(1-u(i))^2*(1-u(i)^((2+lambda)/
    lambda))*(u(i)^((2+3*lambda)/lambda))*abs ...
(mu*(u(i)^(-(lambda+1)/lambda))))/( u(i)^((2+3*lambda)/
    lambda)+ A*(1-u(i))^2*(1-u(i)^((2+lambda)/lambda)))+
    epsilon)/(2*dx^2)+...
(((K/mu_o)*(1-u(i-1))^2*(1-u(i-1)^((2+lambda)/lambda))
    *(u(i-1)^((2+3*lambda)/lambda)) *...
abs( mu*(u(i-1)^(-(lambda+1)/lambda))))/(u(i-1)^((2+3*
    lambda)/lambda)+A*(1-u(i-1))^2*(1-u(i-1)^((2+lambda)
    /lambda)))+epsilon)/(2*dx^2);

D(i,i)= -((((K/mu_o)*(1-u(i+1))^2*(1-u(i+1)^((2+lambda)
    /lambda))*(u(i+1)^((2+3*lambda)/lambda)) *...
abs( mu*(u(i+1)^(-(lambda+1)/lambda))))/(u(i+1)^((2+3*
    lambda)/lambda)+ A*(1-u(i+1))^2*(1-u(i+1)^((2+lambda
```

```
    )/lambda))) ...
+epsilon)/(2*dx^2)+(((K/mu_o)*(1-u(i))^2*(1-u(i)^((2+
    lambda)/lambda))*(u(i)^((2+3*lambda)/lambda))*...
abs(mu*(u(i)^(-(lambda+1)/lambda))))/(u(i)^((2+3*lambda
    )/lambda)+A*(1-u(i))^2*(1-u(i)^((2+lambda)/lambda)))
    +epsilon)/(dx^2) ...
+(((K/mu_o)*(1-u(i-1))^2*(1-u(i-1)^((2+lambda)/lambda))
    *(u(i-1)^((2+3*lambda)/lambda))*...
abs( mu*(u(i-1)^(-(lambda+1)/lambda))))/(u(i-1)^((2+3*
    lambda)/lambda)+ A*(1-u(i-1))^2*(1-u(i-1)^((2+lambda
    )/lambda)))+epsilon)/(2*dx^2));

D(i,i+1)=(((K/mu_o)*(1-u(i))^2*(1-u(i)^((2+lambda)/
    lambda))*(u(i)^((2+3*lambda)/lambda))*...
 abs( mu*(u(i)^(-(lambda+1)/lambda))))/(u(i)^((2+3*
     lambda)/lambda)+ A*(1-u(i))^2*(1-u(i)^((2+lambda)/
     lambda))) ...
 +epsilon)/(2*dx^2)+(((K/mu_o)*(1-u(i+1))^2*(1-u(i+1)
     ^((2+lambda) /lambda))*(u(i+1)^((2+3*lambda)/lambda
     ))*...
 abs( mu*(u(i+1)^(-(lambda+1)/lambda))))/(u(i+1)^((2+3*
     lambda)/lambda)+A*(1-u(i+1))^2*(1-u(i+1)^((2+lambda
     )/lambda)))+epsilon)/(2*dx^2);

end %for i = 2:I-1
end % for n=1:N

u_plot0=u_old*poros;
u_plot=u_new*poros;

%-------------------------------------------------------------------%
% Set output parameters
%-------------------------------------------------------------------%
set(gca,'Color',[1 1 0.9]);
plot(x,u_plot,'-r','LineWidth',3);
axis([0.00 0.4 -0.02 0.4]);
grid on
clear
```

Bibliography

[1] C.J. van Duijn, Y. Fan, L.A. Pelletier, I.S. Pop. *Traveling wave solutions for degenerate pseudo-parabolic equations modelling two-phase flow in porous media*. Elsevier, Nonlinaer Analysis: Real World Applications 14 (2013) 1361-1383.

[2] R.Hilfer, R. Steinle. *Saturation overshoot and hysteresis for twophase flow in porous media*. Eur. Phys. J. Special Topics 223, 2323-2338, (2014).

[3] D.A. Di Carlo, M. Mirzaei, B. Aminzadeh. *Fractional Flow Approach to Saturation Overshoot*. Transp. Porous Med. (2012) 91:955-971 DOI 10.1007/s 11242-011-9885-8.

[4] D.A. Di Carlo. *Experimental measurements of saturation overshoot on infiltration*. Water resources Research Vol 40, W04215, doi: 10.1029/2003WR002670, (2004).

[5] Hassanizadeh, S.M and W.G. Gray, *Thermodynamic basis of capillary pressure in porous media*. Water Resour. Res., 29, 3389-3405, (1993).

[6] Hassanizadeh, S.M., Oung, O., and S. Manthey, *Laboratory experiments and simulations on the significance of non-equilibrium effect in the capillary pressure-saturation relationship, in: Unsaturated Soils: Experimental Studies*. Proceedings of the International Conference: From Experimental Evidence towards Numerical Modeling of Unsaturated Soils, Weimar, Germany, September 18-19, 2003, Volume 1, Ed. T. Schanz, Springer Verlag, Berlin, pp. 3-14, (2004).

[7] Eliassi, M., and R. J. Glass, *On the continuum-scale modeling of gravity-driven fingers in unsaturated porous media: The inadequacy of the Richards' equation with standard monotonic constitutive relations and hysteretic equations of state*. Water Resour. Res., 37, 2019 2035 (2001).

[8] C.J.van Duijn, S.M.Hassanizadeh, I.S.Pop, P.A.Zegeling, *Non-equilibrium Models for Two Phase Flow in Porous Media: the Occurrence of Saturation Overshoots*. ICAPM 2013: Proceedings of the 5th International Conference on Applications of Porous Media, pp. 59 - 70 (2013).

[9] S. Bottero, S.M. Hassanizadeh, P.J. Kleingeld, T.J. Heimovara, *Nonequilibrium capillarity effects in two- phase flow through porous media at different scales*. Water Resour. Res. 47, W10505 (2011).

[10] S. Bottero, *Advances in the theory of capillarity in porous media*. Ph.D. thesis, Geologica Ultreietina, 314, 200 pp, (2009).

[11] B. Plohr, D. Marchesin, P. Bedrikovetsky and P. Krause, *Modeling hysteresis in porous media flow via relaxation*. Computational Geosciences 5: 225256, (2001).

[12] K.Furati, *Effects of relative permeability hysteresis dependence on two-phase flow in porous media*. Transport in Porous Media, vol. 28, pp. 181-203, (1997).

[13] D. Marchesin, H. B. Medeiros and P. J. Paes-Leme, *A model for two-phase flow with hysteresis*. Contemporary Mathematics, vol. 60, pp. 89-107, (1987).

[14] D. Marchesin, H. B. Medeiros and P. J. Paes-Leme, *Hysteresis in two-phase flow: A simple mathematical model*. Comput. Appl. Math., vol. 17, pp. 81-99, (1998).

[15] B. Plohr, D. Marchesin, P. Bedrikovetsky and P. Krause, *Modeling hysteresis in porous media flow via relaxation*. Comput. Geosciences, vol. 5, pp. 225-256, (2001).

[16] P. Bedrikovetsky, D. Marchesin, and P. R. Ballin, *Mathematical model for immiscible displacement honouring hysteresis*. SPE 30132, Fourth Latin American and Caribbean Petroleum Engineering Conference, Port of Spain, Trinidad-Tobago, pp. 557-575, (1996).

[17] W. Hundsdorfer and J. Verwer, *Numerical Solution of Time-Dependent Advection-Diffusion-Reaction Equations*. Vol. 33 of Springer Series in Computational Mathematics. Springer, Berlin, (1993).

[18] F. M. van Kats and C. J. Van Duijn, *A Mathematical Model for Hysteretic Two-Phase Flow in Porous Media*. Transport in Porous Media 43: 239263, Department of Mathematics, Delft University of Technology, Mekelweg 4, 2628 CD Delft, The Netherlands, (2001).

[19] MathWorks, *Matrix inverse*. (1994-2016) http://nl.mathworks.com/help/matlab/ref/inv.html?refresh=true.

[20] Brooks, R.H., and A. T. Corey, *Hydraulic properties of porous media*. Hydrology Paper No. 3, Colorado State University, 3:127, (1964).

[21] Lawrence C. Evans, *Partial Differential Equations: Second Edition*. University of California, Berkeley, Volume: 19 2010 749 pp; Softcover MSC: Primary 35; Secondary 49; 47, (2010).

[22] Graham Griffiths and William E. Schiesser, *Traveling Wave Analysis of Partial Differential Equations*. Elsevier Science Publishing, Co Inc, March, (2011).

[23] C. J. van Duijn, Y. Fan, L. A. Peletier and I. S. Pop, *Travelling wave solutions for a degenerate pseudo-parabolic equation modelling two-phase flow in porous media*. Nonlinear Anal. Real World Appl, 1361-1383, (2013).